WADD TECHNICAL REPORT 60-190

ELECTRON BEAM TECHNIQUE FOR MEASURING THE THERMOPHYSICAL PROPERTIES OF MATERIALS

H. M. CHILDERS
J. M. CERCEO

AMERICAN MACHINE & FOUNDRY COMPANY
ALEXANDRIA, VIRGINIA

APR 1 1 1962

CONTRACT Nr. AF 33(616)-6527

NOVEMBER 1961

PHYSICS LABORATORY
AERONAUTICAL SYSTEMS DIVISION
AIR FORCE SYSTEMS COMMAND
UNITED STATES AIR FORCE
WRIGHT-PATTERSON AIR FORCE BASE, OHIO

contrails.iit.edu

NOTICES

When Government drawings, specifications, or other data are used for any purpose other than in connection with a definitely related Government procurement operation, the United States Government thereby incurs no responsibility nor any obligation whatsoever; and the fact that the Government may have formulated, furnished, or in any way supplied the said drawings, specifications, or other data, is not to be regarded by implication or otherwise as in any manner licensing the holder or any other person or corporation, or conveying any rights or permission to manufacture, use, or sell any patented invention that may in any way be related thereto.

Qualified requesters may obtain copies of this report from the Armed Services Technical Information Agency, (ASTIA), Arlington Hall Station, Arlington 12, Virginia.

This report has been released to the Office of Technical Services, U. S. Department of Commerce, Washington 25, D. C., for sale to the general public.

Copies of ASD Technical Reports and Technical Notes should not be returned to the Aeronautical Systems Division unless return is required by security considerations, contractual obligations, or notice on a specific document.

ELECTRON BEAM TECHNIQUE FOR MEASURING THE THERMOPHYSICAL PROPERTIES OF MATERIALS

H. M. CHILDERS
J. M. CERCEO

AMERICAN MACHINE & FOUNDRY COMPANY

NOVEMBER 1961

AERONAUTICAL SYSTEMS DIVISION
AIR FORCE SYSTEMS COMMAND
UNITED STATES AIR FORCE
WRIGHT-PATTERSON AIR FORCE BASE, OHIO

FOREWORD

ABSTRACT

The determination of the suitability of electron bombardment for measuring the thermophysical properties of materials is made. A solution is given which is applicable to the case of a radiating cylindrical sample. Conclusions are that the technique offers a valuable tool for measuring these properties within described limits. Values of α, k, ρc_p, and ε were determined for graphite and Al_2O_3 (Polycrystalline). Recommendations on instrumentation are made for the further development of this technique.

PUBLICATION REVIEW

This report has been reviewed and is approved.

For the Commander:

Jules I. Wittebort
Chief, Thermophysics Branch
Thermodynamics Section
Physics Laborabory

iii

CONTENTS

LIST OF ILLUSTRATIONS

LIST OF ILLUSTRATIONS (continued)

LIST OF TABLES

SYMBOLS

A = Cross sectional area.

c_p = Specific heat at constant pressure.

f = Frequency of the temperature wave.

f_m = Maximum frequency of the temperature wave.

k = Thermal conductivity (cgs).

n = Statistical degrees of freedom.

P = Power = $\partial Q / \partial t$.

P_c = Power conducted across the sample.

P_r = Power radiated from the front face.

$P(t)$ = Total power input = $P_r + P_c$.

P_m = Maximum power input.

P_o = Steady state power input.

P_{of} = Steady state power radiated from front face.

P_{os} = Steady state power radiated from back face.

Q = Heat energy/ unit area.

S = Sample thickness.

$T(x, t)$ = Temperature as a function of time and distance.

T_b = Black body temperature.

T_s = Sample temperature.

T_{os} = Steady state temperature of back face of sample.

T_{osb} = Steady state black body temperature of back face.

T_{ofb} = Steady state black body temperature of front face.

T = Temperature in degrees Kelvin.

T_f = Maximum temperature variation about the average.

T_{of} = Steady state temperature of front face.

T_{af} = Statistical average front face temperature.

T_{ab} = Statistical average back face temperature.

T_{as} = Statistical average sample temperature = $\dfrac{T_{af} + T_{ab}}{2}$.

t = Time in seconds.

$\underline{\text{grad}}\ T = \nabla T$ = gradient of $T = \dfrac{\partial T}{\partial x}$ (for one dimensional case in x direction).

V = Wave velocity = $dx/dt = \sqrt{2\alpha\omega}$.

ΔW = $\left[\sigma T_{of}^4 - \sigma(T_{of} - T_f)^4\right]$

x = Distance in centimeters.

α = Thermal diffusivity (cgs).

Δ = Parameter difference, ex: $(T_{as_2} - T_{as_1}) = \Delta T_{as}$.

ϵ = Total normal emissivity.

λ = Wave length of temperature wave.

ρ = Sample density gm cm^{-3}.

σ = Stefan - Boltzman constant.

τ = Wave period = $1/f$.

ϕ = Temperature wave phase shift front to back.

ω = Angular frequency = $2\pi f$.

ω_m = Maximum angular frequency = $2\pi f_m$.

I. INTRODUCTION

The present trend in materials technology places increasing
demands upon the present reservoir of data concerning the thermophysi-
cal properties of materials. Research on instrumentation and tech-
niques will render such data more readily available. Since data is es-
pecially scarce at high temperatures, there is need for techniques whose
high temperature limitations are determined by the melting or decompo-
sition temperatures of the materials. It is therefore the purpose of this
report to describe one such technique in which the heat energy is trans-
ferred to the material by electron bombardment.

The purpose of the present investigation was to experimentally
establish the feasibility of determining the thermal diffusivity, thermal
conductivity, heat capacity, and emissivity of materials through use of
an electron beam to heat the sample. The technique involves controlling
the temperature variations of one face of a cylindrical sample in a pre-
determined manner. The application depends upon the fact that, if the
sample specimen is suspended in a vacuum in such a manner that there
is essentially no conductive heat energy losses, the boundary conditions
will be determined by the electron beam power input and the radiation
losses. Since the surface conditions of the sample material can be

controlled and since the surface temperatures can be measured, the temperature behaviour of the sample boundaries can be specified. With these boundary conditions, it is possible to obtain a unique solution to the associated differential equation which specifies the temperature behaviour of the sample in terms of the thermophysical parameters, thermal diffusivity α, thermal conductivity k, specific heat c_p, and total normal emissivity ϵ.

In the first section of this report, the solution of the problem is given for a sinusoidal temperature variation on one face of a right circular cylindrical sample. The conditions are then established for determining the thermal diffusivity of the sample from periodic steady state conditions. By observing the relative temperatures of the two faces of the sample for steady heating, a second independent relationship between the four thermophysical parameters is obtained. If the temperature on one of the faces is determined, a relationship between the emissivity and the apparent black body temperature is obtained. Finally, if advantage is taken of the defined relationship between the thermal diffusivity, thermal conductivity, and heat capacity, a fourth simultaneous equation is obtained from which all four of the thermophysical parameters can be determined.

The next section of the report gives a description of the experimental apparatus. Since only a feasibility study was intended no effort was made to develop a refined apparatus.

The third section of the report gives a description of the experiment and the results. The power input was hand-operated throughout the experimental work. Because the measurements require precise control and the human response time is rather long, only a very limited range of temperatures and materials was investigated. Results are presented for graphite and alumina samples.

The fourth section of the report discusses the technique and presents conclusions concerning its utility. It is concluded that the technique can be instrumented so that it will represent a valuable contribution to high-temperature technology. The chief advantage of the technique is that all four of the thermophysical constants can be measured over a large temperature range and for a wide variety of materials.

The final section of the report makes recommendations for the development of improved instrumentation for application of this particular technique. Such instrumentation would be more easily operated than existing equipment which can accomplish similar results, and would be competitive from an economical point of view.

II. THEORY

The problem of heat transfer for the case of the uniformly heated plane of finite thickness, extending to infinity in the z and y directions can be solved approximately. For large values of time when the body is at a steady temperature of T_s, the power radiated at the back surface is given by $P_r = \epsilon \sigma T_s^4$. If periodic steady state variations are superimposed on this (i.e., after the transients have died out) the variations in radiated power at the back surface will then be given by

$$\Delta P_r = \epsilon \sigma \left\{ (T_s + \theta)^4 - T_s^4 \right\}, \tag{1}$$

where θ is the steady state periodic temperature variation. The expansion of equation (1) gives

$$\Delta P_r = \epsilon \sigma \left[4 T_s^3 \theta + 6 T_s^2 \theta^2 + 4 T_s \theta^3 + \theta^4 \right], \tag{2}$$

which, for $\theta << T_s$, can be closely approximated by

$$\Delta P_r \cong 4 \epsilon \sigma T_s^3 \theta. \tag{3}$$

If the steady state periodic temperature variation on the heated side of the plane is forced to vary in a sinusoidal manner by proper control of the power input at that surface then all of the boundary conditions of interest are known. The differential equation of heat transfer for a slab of thickness $o \leq x \leq \ell$ with heat input at $x = o$, is

$$\frac{\partial^2 \theta}{\partial x^2} = \frac{1}{\alpha} \frac{\partial \theta}{\partial t} \quad o < x < \ell \tag{4}$$

The corresponding boundary conditions are

$$\theta = V \cos \omega t \text{ at } x = o, \tag{5}$$

$$-k \frac{\partial \theta}{\partial x} = h\theta \text{ at } x = \ell. \tag{6}$$

Here $h = 4\epsilon\sigma T_s^3$, k is the thermal conductivity, and

$$\theta(x, t) = 0 \text{ for } t \le 0. \tag{7}$$

The Laplace transforms of 4, 5, and 6, are,

$$\frac{d^2\bar{\theta}}{dx^2} - q^2\bar{\theta} = 0 \qquad 0 < x < \ell \tag{8}$$

where $q^2 = p/\alpha$ $\bar{\theta} = \int_0^\infty e^{-pt}\theta(x, t)\,dt$, $\alpha = k/\rho C_p$ is the thermal

diffusivity, ρ is the density and C_p is the specific heat,

$$\bar{\theta}(x, p) = V \frac{p}{p^2 + \omega^2} \text{ for } x = 0, \tag{9}$$

and

$$-k \frac{d\bar{\theta}}{dx} = h\bar{\theta} \text{ for } x = \ell. \tag{10}$$

The general solution of equation (8) is

$$\bar{\theta}(x, p) = A e^{qx} + B e^{-qx} \qquad 0 < x < \ell; \tag{11}$$

so that

$$\frac{d\bar{\theta}}{dx} = q(A e^{qx} - B e^{-qx}) \qquad 0 < x < \ell, \tag{12}$$

and by 9 and 10,

$$-kq(A e^{q\ell} - B e^{-q\ell}) = h(A e^{q\ell} + B e^{-q\ell}) \qquad x = \ell, \tag{13}$$

and

$$A + B = V \frac{p}{p^2 + \omega^2}. \tag{14}$$

Equations 13 and 14 allow us to solve for A and B, the solutions being

$$A = V \frac{p}{p^2 + \omega^2} e^{-q\ell} \left[\frac{kq - h}{2kq \cosh q\ell + 2h \sinh q\ell} \right], \tag{15}$$

5

and

$$B = V \frac{p}{p^2 + \omega^2} e^{q\ell} \left[\frac{kq + h}{2kq \, Cosh \, q \, + 2h \, Sinh \, q\ell} \right].$$ (16)

Equation 11 can then be written

$$\bar{\theta}(x, p) = V \frac{p}{p^2 + \omega^2} \left[\frac{2kq \, Cosh \, q(\ell - x) + 2h \, Sinh \, q(\ell - x)}{2kq \, Cosh \, q\ell + 2h \, Sinh \, q \ell} \right],$$ (17)

whose solution for $\theta(x, t)$ is given by

$$\theta(x, t) = \frac{1}{2\pi j} \int_{\gamma - j\infty}^{\gamma + j\infty} e^{pt} \bar{\theta}(x, p) \, dp$$ (18)

where all singularities lie to the left of the line $(\gamma - j\infty, \gamma + j\infty)$. For a function which is analytic in the region of interest, except at a finite number of poles, the contour integral representing equation 18 can be shown by Cauchy's theorem to be

$$\theta(x, t) = \Sigma \, Res.$$ (19)

The poles of interest for the steady state periodic case are along the imaginary axis at $\pm j\omega$ and hence the inverse transform of 17 is

$$\theta(x, t) = \lim_{p \to j\omega} \left\{ \frac{Ve^{pt} \omega(p - j\omega)}{(p + j\omega)(p - j\omega)} \left[\frac{2kq \, Cosh \, q(\ell - x) + 2h \, Sinh \, q(\ell - x)}{2kq \, Cosh \, q\ell + 2h \, Sinh \, q\ell} \right] \right. +$$

$$+ \lim_{p \to -j\omega} \left\{ \frac{Ve^{+pt} \omega(p + j\omega)}{(p + j\omega)(p - j\omega)} \left[\frac{2kq \, Cosh \, q(\ell - x) + 2h \, Sinh \, q(\ell - x)}{2kq \, Cosh \, q\ell + 2h \, Sinh \, q\ell} \right] \right..$$ (20)

Defining the quantities $\beta = \sqrt{\frac{\omega}{2\alpha}}$, $b = \beta(1 + j)$, $b^* = \beta(1 - j)$, equation 20 can be written

$$\theta(x, t) = \frac{Ve^{j\omega t}}{2} \left[\frac{2kb \, Cosh \, b(\ell - x) + 2h \, Sinh \, b(\ell - x)}{2kb \, Cosh \, b\ell + 2h \, Sinh \, b \ell} \right] +$$

$$\frac{Ve^{-j\omega t}}{2} \left[\frac{2kb^* \, Cosh \, b^*(\ell - x) + 2h \, Sinh \, b^*(\ell - x)}{2kb^* \, Cosh \, b^*\ell + 2h \, Sinh \, b^*\ell} \right],$$ (21)

6

which can be shown to satisfy the differential equation (4) and the boundary conditions of equations 5, 6, 7. It can be shown that at the back face $(x = \ell)$ equation (21) has the form

$$\theta(\ell, t) = \frac{V}{2C} \{(a' + ja'') e^{j\omega t} + (a' - ja'') e^{-j\omega t}\} , \tag{22}$$

where

$$a' = 8k^2 \beta^2 \, Cosh\, \beta\ell \, Cos\, \beta\ell + 4kh\, \beta\, Sinh\, \beta\ell\, Cos\, \beta\ell + 4kh\, \beta\, Cosh\, \beta\, Sin\, \beta\ell,$$

$$a'' = 8k^2 \beta^2 \, Sinh\, \beta\ell\, Sin\, \beta\ell + 4kh\, \beta\, Sinh\, \beta\ell\, Cos\, \beta\ell - 4kh\, \beta\, Cosh\, \beta\ell\, Sin\, \beta\ell,$$

and $C = (2kb\, Cosh\, b\, \ell + 2h\, Sinh\, b\ell)(2kb^*\, Cosh\, b^*\ell + 2h\, Sinh\, b^*\ell).$

Substituting for the exponentials in equation 22, we have

$$\theta(\ell, t) = \frac{V}{C} [a'\, Cos\, \omega t - a''\, Sin\, \omega t] \tag{23}$$

which has the form

$$\theta(\ell, t) = \frac{V}{C} [Cos\, (\omega t - \phi)] \tag{24}$$

with $a' = Cos\, \phi$, and $-a'' = Sin\, \phi$. The phase angle ϕ is then specified by

$$\tan \phi = \frac{Sin\, \phi}{Cos\, \phi} = -\frac{a''}{a'} \tag{25}$$

or

$$\phi = \tan^{-1} \left[\frac{2k\, \beta\, Sinh\, \beta\ell\, Sin\, \beta\ell - h(Sinh\, \beta\ell\, Cos\, \beta\ell - Cosh\, \beta\ell\, Sin\, \beta\ell)}{2k\, \beta\, Cos\, h\, \beta\ell\, Cos\, \beta\ell + h(sinh\, \beta\ell\, Cos\, \beta\ell + Cosh\, \beta\ell\, Sin\, \beta\ell)} \right] \tag{26}$$

Equation 26 can be rewritten,

$$\phi = \tan^{-1} \left[\frac{\tanh \beta\ell\, \tan \beta\ell - (K/\beta\ell)\, [\tanh \beta\ell - \tan \beta\ell]}{1 + (K/\beta\ell)[\tanh \beta\ell + \tan \beta\ell]} \right] , \tag{27}$$

where $K = \ell h/2k$. For $2(k/\ell) \gg h$, i.e., for $K \ll 1$, radiation losses, ΔP_r, at the back face can be neglected and equation 27 reduces to

7

$$\phi = \tan^{-1} [\tanh \beta l \tan \beta l]. \tag{28}$$

Figure 1 shows a graph of ϕ vs βl for equations 27 and 28 with K = 0.147, this choice being more stringent than the most severe experimental case considered. The curve shows that for βl = 1.6 rad, the tanh βl factor introduces only 8% deviation in tan ϕ from that of the solution for the semi-infinite medium (for small values of h) and rapidly converges to $\phi = \beta l$. If the radiation loss effects are accounted for in equation 27, it is seen that for the case of Al_2O_3 mentioned the terms containing h result in smaller values of ϕ from those given by equation (28).

For the assumption made in equation (3), i.e., $T_s \gg \theta$, if the amplitude is $\theta = 0.05 \, T_s$, values of θ can be as large as $\pm 70^\circ$K at 1400°K which is ample for detection. Equation (2) then becomes, at the maximum,

$$\Delta P_r = \epsilon \sigma T_s^4 [0.20 + 0.015 + 0.000125 + 0.000006].$$

By discarding second order terms in θ a total error in ΔP_r of 7.75% is then introduced. However, optimum conditions can be chosen to reduce this error such as smaller values of θ_{max} and larger values of βl.

The radiation losses at the front face are compensated for in the power input by the inclusion of the sine wave temperature form in the front face boundary conditions. The assumption of linear heat transfer through the sample can be justified in the choice of the experimental arrangement, i.e., $l \ll r$, where r is the radius of the disk, and by
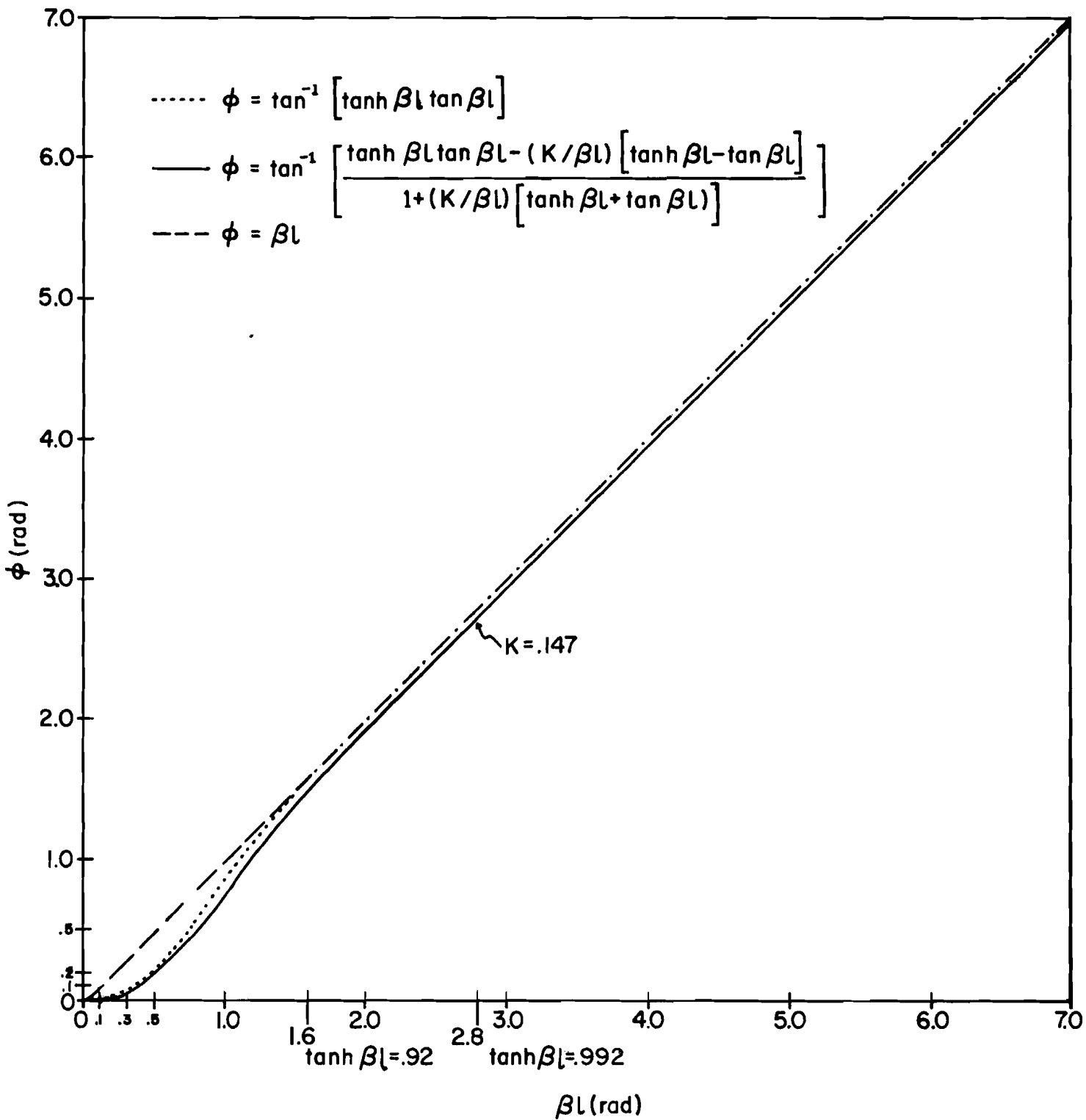
FIG. 1 ϕ vs βl

9

radiation shielding at the sides of the sample. However, the assumption of equation (6) can equally well be applied at all surfaces of the sample in the solution of the general form of the differential equation $\frac{\partial \theta}{\partial t} = \alpha \nabla^2 \theta$. This could be done as a further check on the experimental imposition of linear heat transfer in the sample.

A determination of emissivity as a function of temperature can be made by use of a thermocouple which measures absolute temperature, a radiometer which measures black body temperature, and the relation

$$P_s / P_B = \epsilon_s , \tag{29}$$

where P_B is the apparent black body power radiated from the sample. The conductivity can be obtained from the steady nonperiodic temperature gradient. The boundary condition is, for steady heating,

$$\frac{k}{\ell} [T_f - T_b] = \epsilon \sigma T_b^4 , \tag{30}$$

where T_f and T_b are the front and back face temperatures respectively, and k is the only unknown. The sample density, ρ, can be determined easily by a measure of mass and volume, and specific heat can be determined from

$$C_p = k / \rho \alpha. \tag{31}$$

Throughout the discussion it has been assumed that the temperature dependence of α is small because θ is small. For steady, nonperiodic measurements this is not a problem.

III. EXPERIMENTAL APPARATUS

The equipment required to perform these experiments can be separated into three groups--the test chamber, the power and control apparatus, and the measuring equipment. The test chamber was designed and built providing electrical inlets for the electron gun, access ports for changing samples, and viewing ports for making measurements of the thermophysical properties of the sample while effecting high vacuum conditions. A high voltage supply was designed and built to satisfy the power input requirement necessary to heat the sample. In addition other standard power supplies were used to provide control and focus of the electron beam. Upon completion of construction of the special equipment several methods of measuring the thermophysical properties of materials were investigated using a photocell and a radiometer.

A. TEST CHAMBER

The test chamber, shown schematically in Figures 2 and 3, was constructed from a 6-inch standard welding pipe cross with 6-inch welding flanges. All parts of the chamber and fittings were sandblasted and welded, followed by polishing and tinning the welds. All the sealing surfaces were cleaned and polished and provided with "O" rings wherever possible. Water cooling coils were soldered to the chamber to prevent heating of the chamber. Later, in actual operation, the coils were
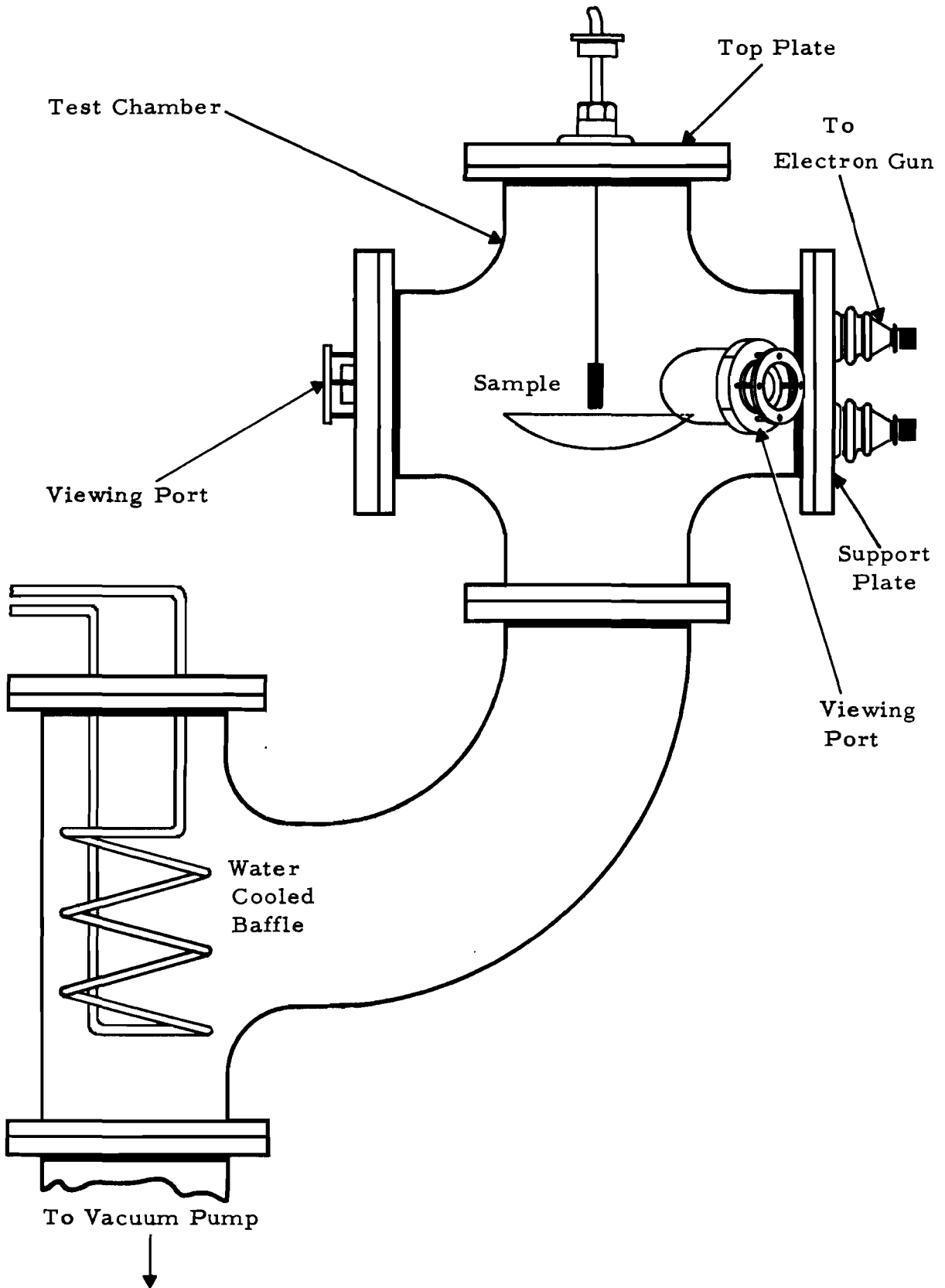
Figure 2   Schematic, Over-all Test Chamber.

Radiation Detector

Port to Vacuum Pump

Viewing Port

Support Plate

Viewing
Port

Electron
Gun

Cooling Coils

Viewing Port

Sample (Suspended From Top Plate)

Radiation Detector
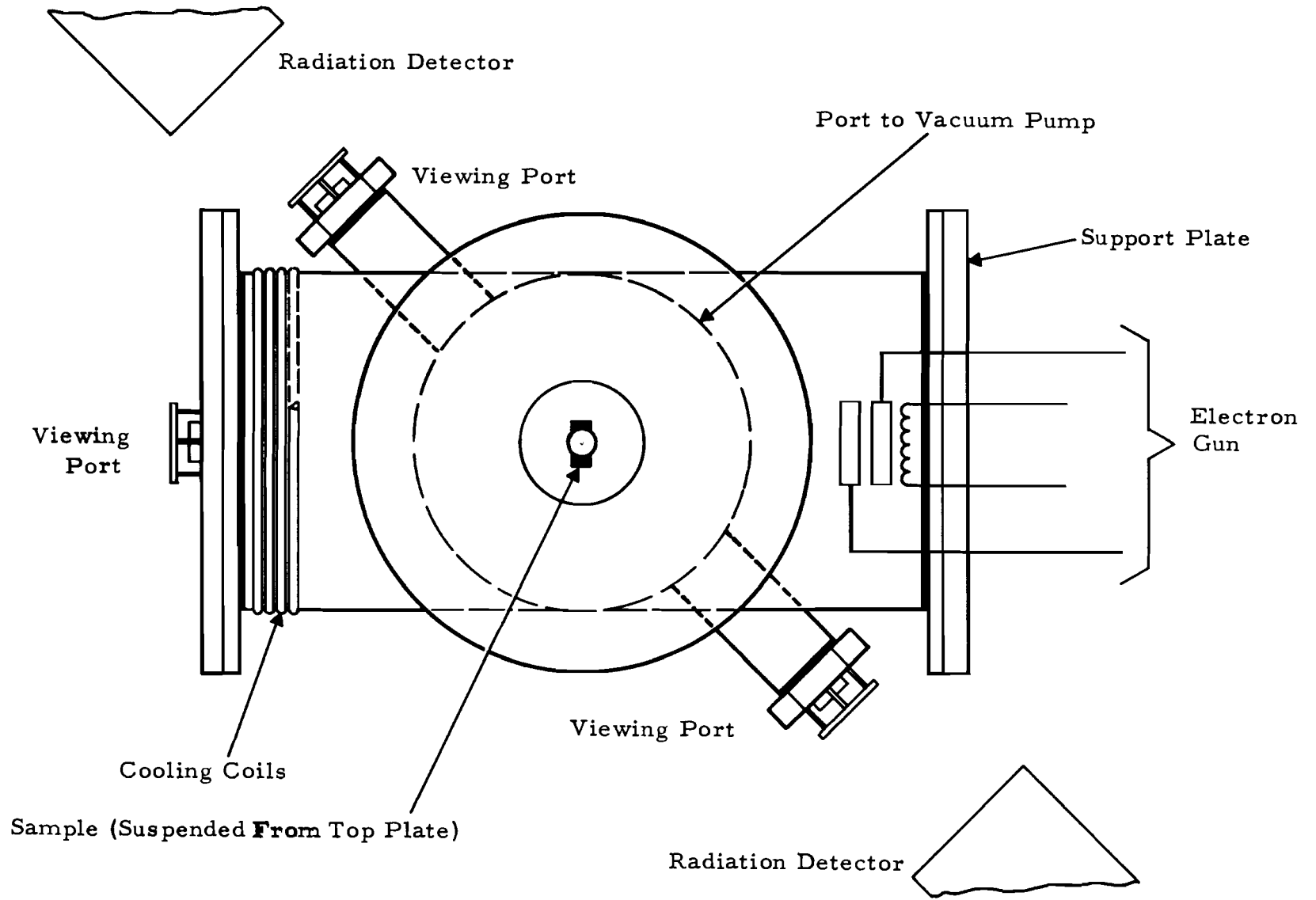
Figure 3   Schematic, Top View of Test Chamber

found to be unnecessary because the chamber walls remained at room temperature.

In order to obtain the vacuum and the pumping speed required to exceed outgassing of the samples at elevated temperatures, a mechanical pump and an oil diffusion pump were used. The mechanical pump was a Kinney type KC-15 having a capacity of 15 CFM. A 6-inch Consolidated Engineering Corp. MCF-700 oil diffusion pump was used in conjunction with the Kinney pump. A water cooled baffle (shown in Figure 2) was provided for the oil diffusion pump. A Phillips Ionization Gauge and a thermocouple gauge were mounted into the system. Figure 4 is a photograph showing the test chamber in place with the associated vacuum pumps (on the right is a view of the 10,000 volt power supply). The best vacuum achieved with this system was approximately 10^{-6} mm of Hg whereas measurements were taken at a pressure of approximately 10^{-5} mm of Hg.

The electron gun (Figure 5) consisted of a filament, a focusing electrode, and an accelerating electrode. Figure 5 shows a view of the interior of the test chamber with the electron gun in place. The filament windings were made of tungsten and arranged in the configuration shown in Figure 6 which is a close-up of the electron gun mounted on heat-treated lava supports. Two coaxial rings were placed in front of the filament to provide focusing and acceleration for the electron beam. The

TEST CHAMBER
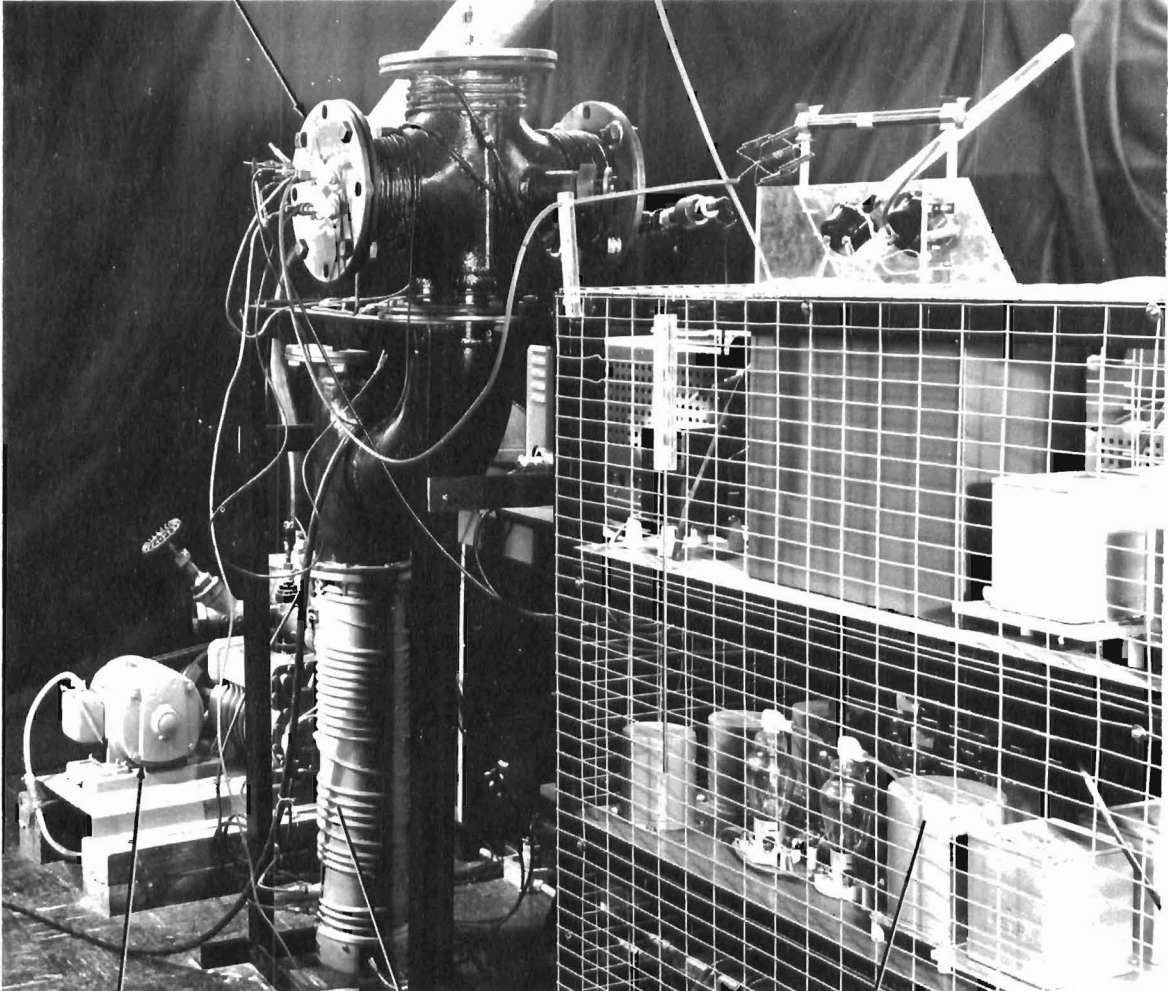
MECHANICAL PUMP   OIL DIFFUSION PUMP   HIGH VOLTAGE POWER SUPPLY

Figure 4. Closeup of Power Supply, Test Chamber, and Vacuum
        Pumps.

15

ELECTRON GUN

VIEWING PORT
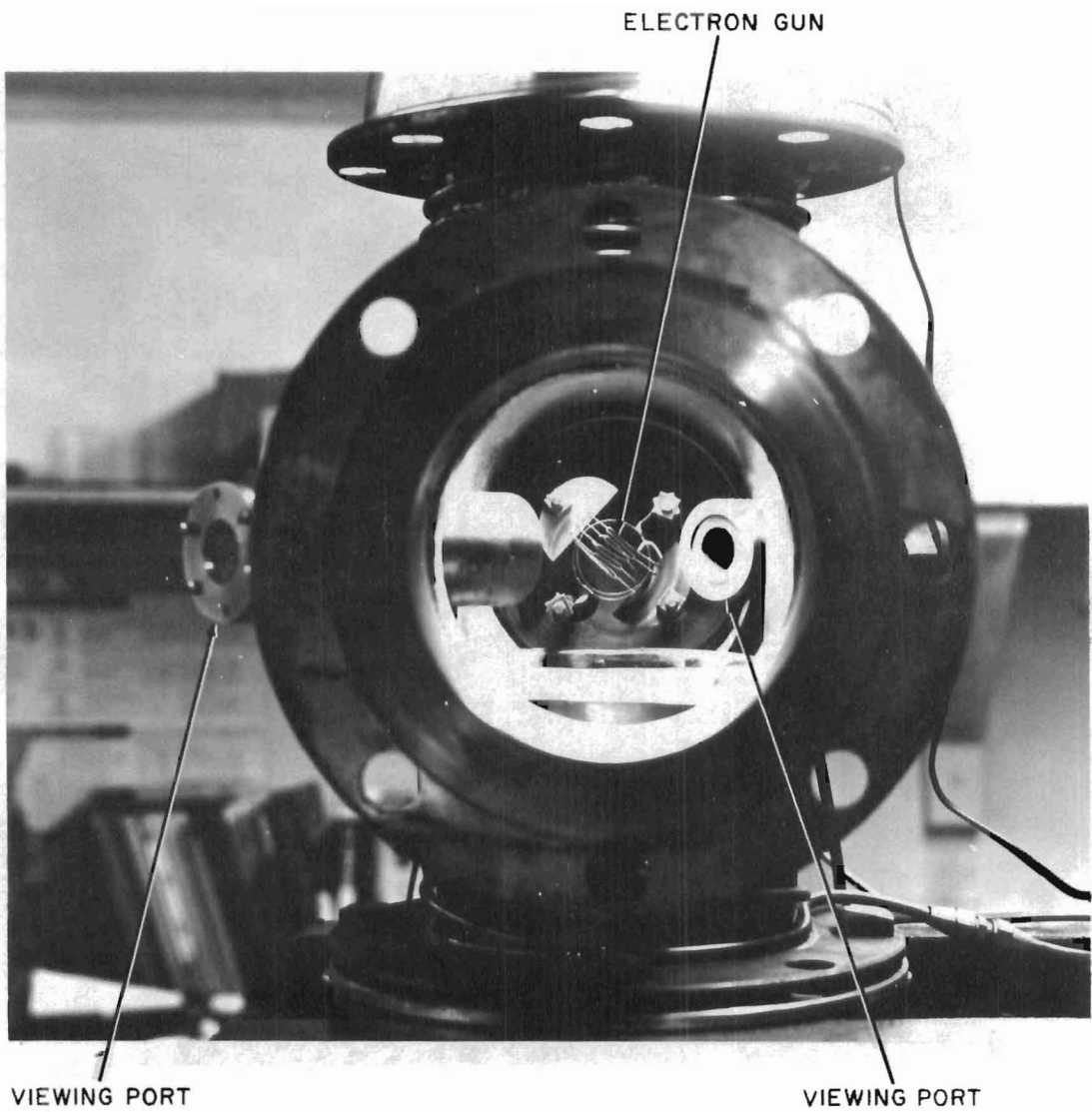
VIEWING PORT

Figure 5. End View of Test Chamber.
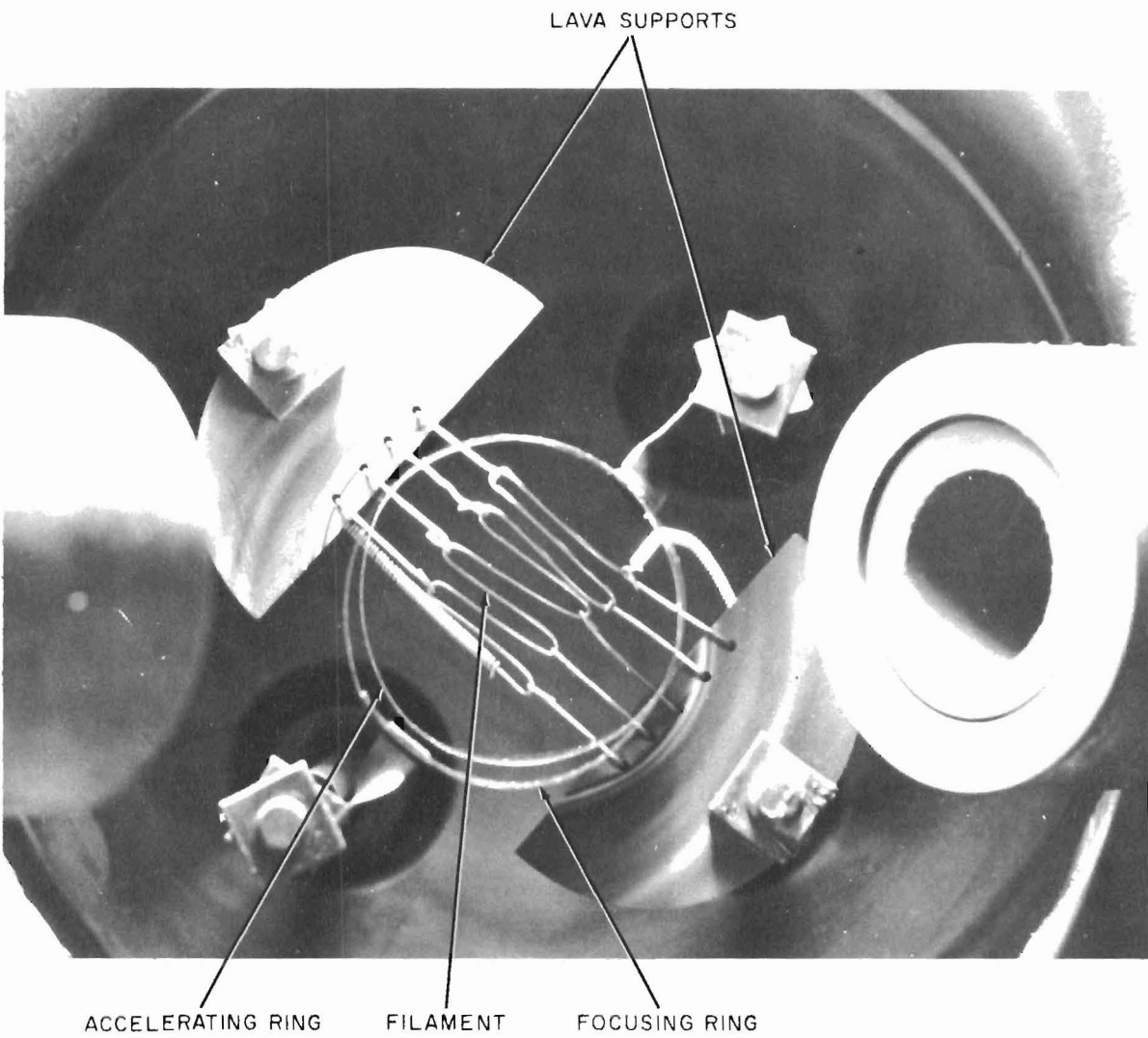
Figure 6. Closeup of Electron Source.

17

power for the electron gun was transferred through the support plate as shown diagrammatically in Figure 7.

The viewing ports from which the measurements were made can be seen in Figure 5 as cylindrical tubes projecting obliquely into the chamber. The viewing ports were terminated with $\frac{1}{2}$ inch quartz windows. As indicated in Figures 2 and 3, the sample is seen from a horizontal position through the two viewing ports set at 45° to the longitudinal axis of the cross. Each of the ports was constructed to retain an "O" ring seal for the quartz window and provided a mounting bracket for a radiation measuring device.

The sample was suspended from the top flange by means of a nickel rod and a tungsten wire attached to a molybdenum ring which was rigidly clamped around the edge of the sample. The high voltage was brought through the top flange to the sample by means of a high voltage insulated lead and a special adapter. The special adapter provided rotational and translational (in the vertical direction) freedom of the sample so that it could be centered in the electron beam and oriented into view as seen through the viewing ports.

It may be noted that the contribution to the heat conduction, front to back, provided by the molybdenum ring is negligible compared to the heat conduction through the sample, the reason being that the cross-sectional area presented to the beam by the ring is 10^{-5} times as large as

Standoff Insulators

Support
Plate

Nickel Rods
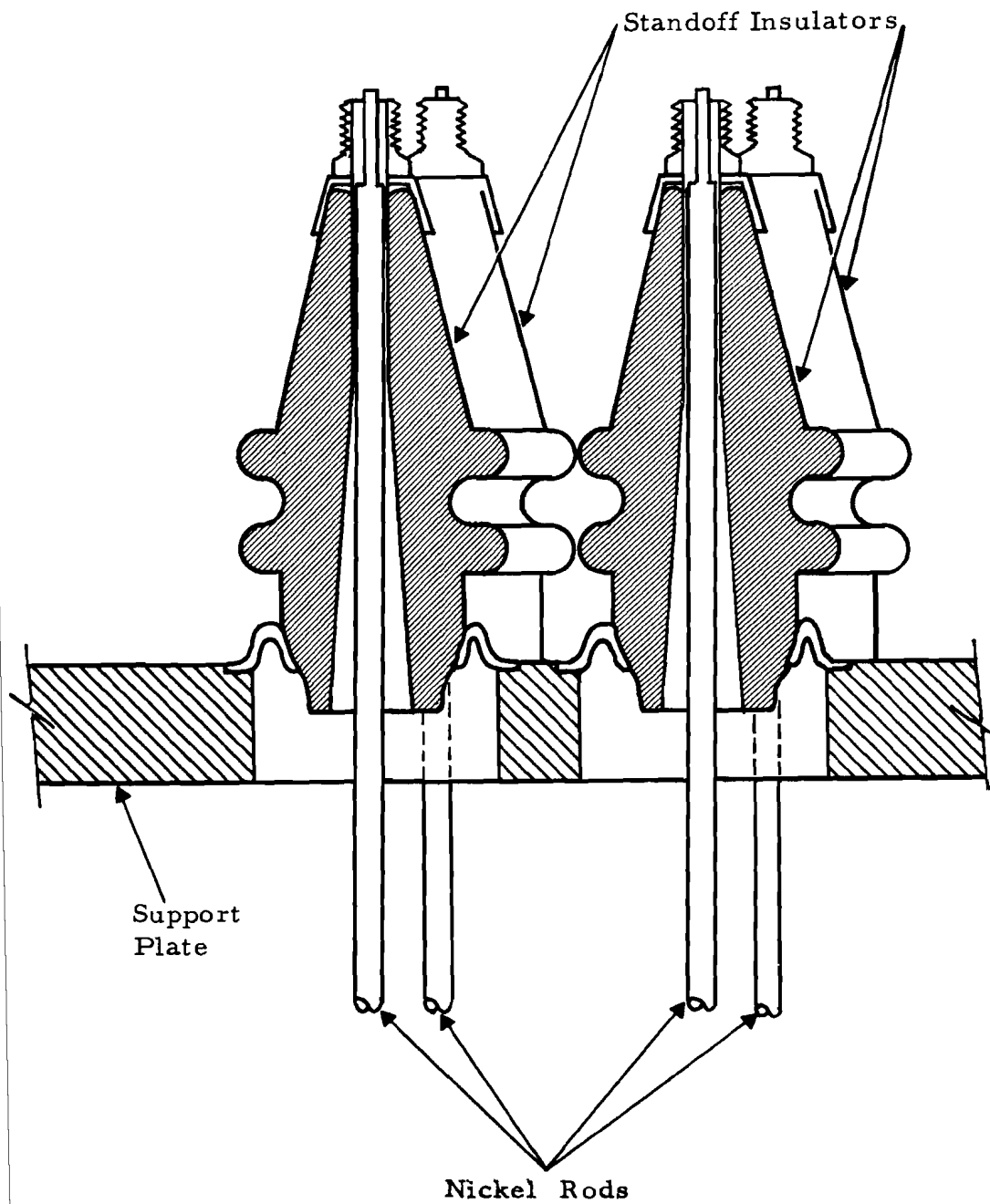
Figure 7. Diagram of Insulator Design on Electron Gun Flange.

the cross-sectional area of the sample. Therefore, heat is transferred to the ring by conduction through the sample.

B. POWER AND CONTROL EQUIPMENT

1. Plate Supply

Because of the high temperatures and uniform heating required in this experiment a high voltage power supply was designed which maintained high stability with low ripple. The high voltage power supply shown schematically in Figure 8 consists principally of three cascaded full wave rectifiers. Each full wave rectifier has a low pass double-L choke-input filter capable of delivering 200 milliamperes of current at 3500 volts dc. The cascaded voltage is then fed to a low pass single-L choke-input filter. When the system was tested across a water load the output was found to be 170 milliamperes at 10,000 volts dc.

To insure low ripple, the ripple voltage superimposed on the dc voltage was measured in the laboratory as shown in the block diagram in Figure 9. The water load represented a pure resistance load to the power supply and simulated actual operating conditions. The use of a blocking capacitor in the oscilloscope input lead permitted the oscilloscope to exhibit high sensitivity for the ripple measurements. The percentage ripple voltages measured at 5000, 7500, and 10,000 volts dc were 0.0032, 0.0053, and 0.0080 percent, respectively.
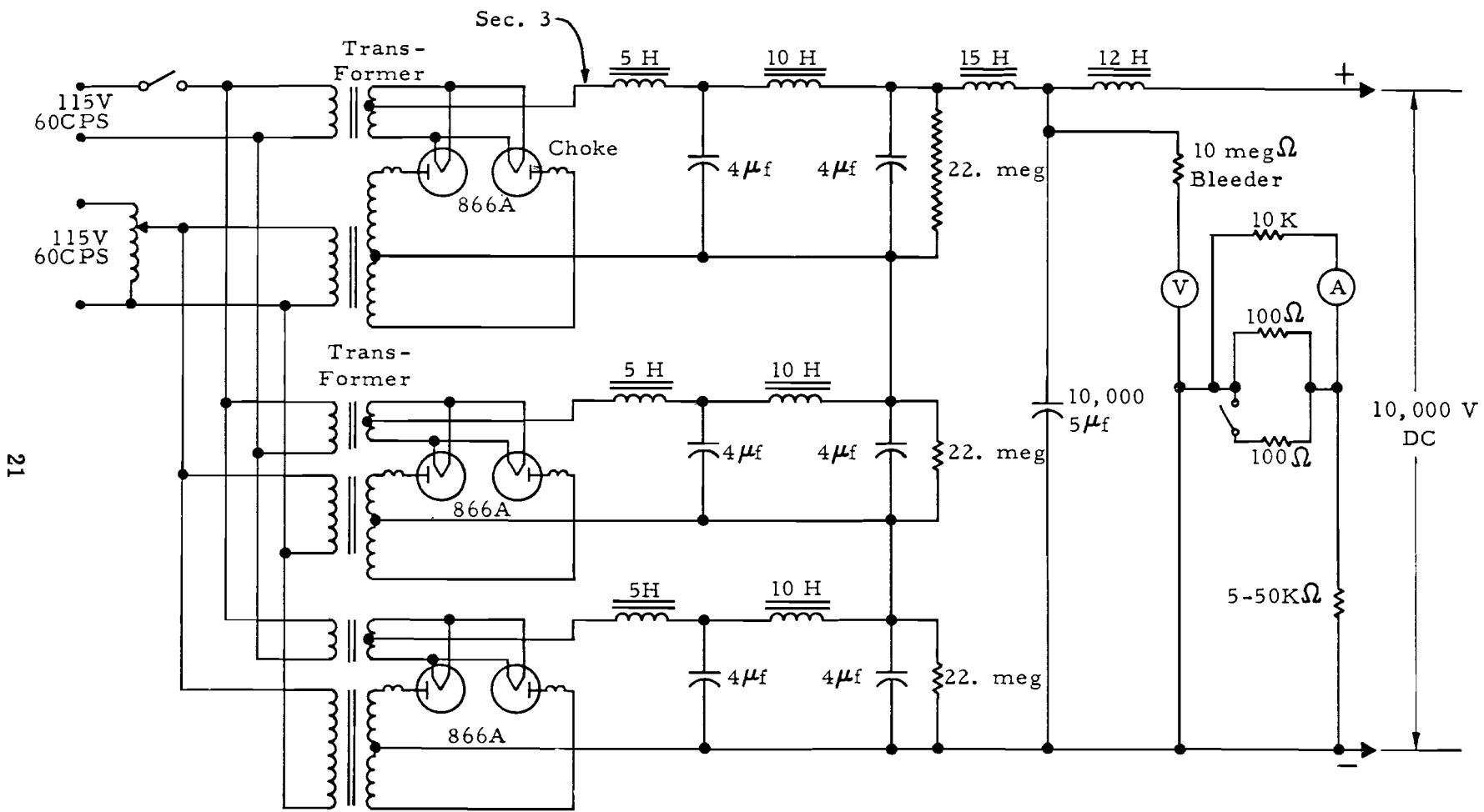
Figure 8. Schematic Diagram of High Voltage Power Supply.

21

15 H

15,000V
500 μμf

Power
Supply
Output
First Stage

10,000V
5 μf

Water
Load

Scope

1 meg
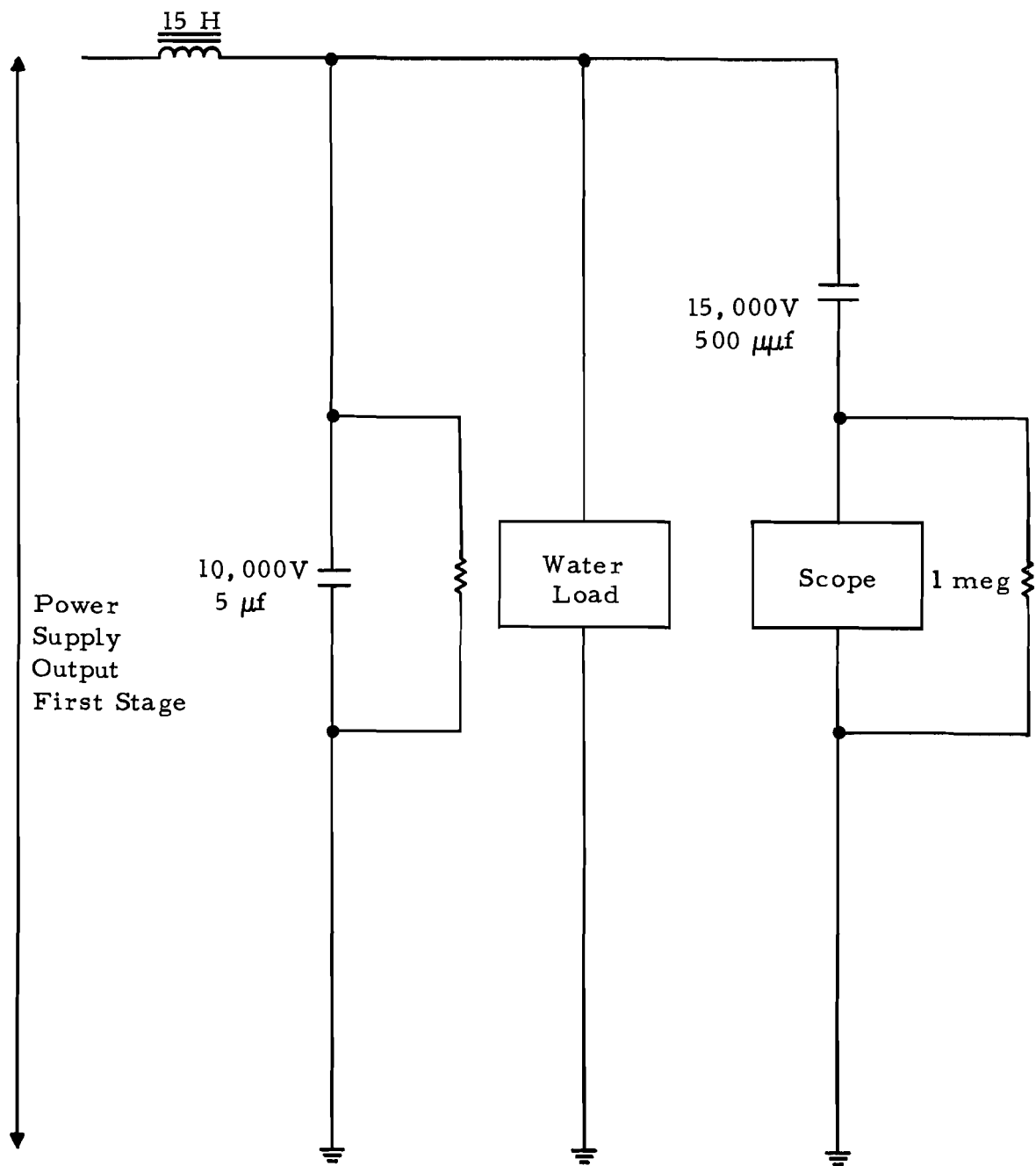
Figure 9. Block Diagram of Ripple Test.

The metering circuit is shown schematically in Figure 10. The measurement and control of the power input to the sample was obtained through the observation of the readings on the meters as shown in Figure 10.

2. Focus and Accelerating Electrode Supplies

The power supplies used to establish a positive voltage on the focus and accelerating electrodes were standard Sorenson supplies, model 600-B. Both proved to be quite useful in establishing control of the beam size and in obtaining a uniform distribution of bombarding electrons over the surface of the sample.

3. Filament Supply

In the initial investigation of this program, modulating frequencies of approximately 5 cps were considered which necessitated the use of extremely stable filament voltage supplies. This degree of stability was supplied by four 12-volt Deka batteries. Control was maintained by building a bank of load resistors, made of Nichrome wire, which were switched into the circuits as desired. Fine control was obtained by using a rheostat which was always in the circuit. A schematic diagram of the filament power supply is shown in Figure 11.

Since in subsequent investigations modulation frequencies were 1 cycle per second or less, the filament power supply was replaced by a 16 volt 17 amp transformer. A considerable advantage in
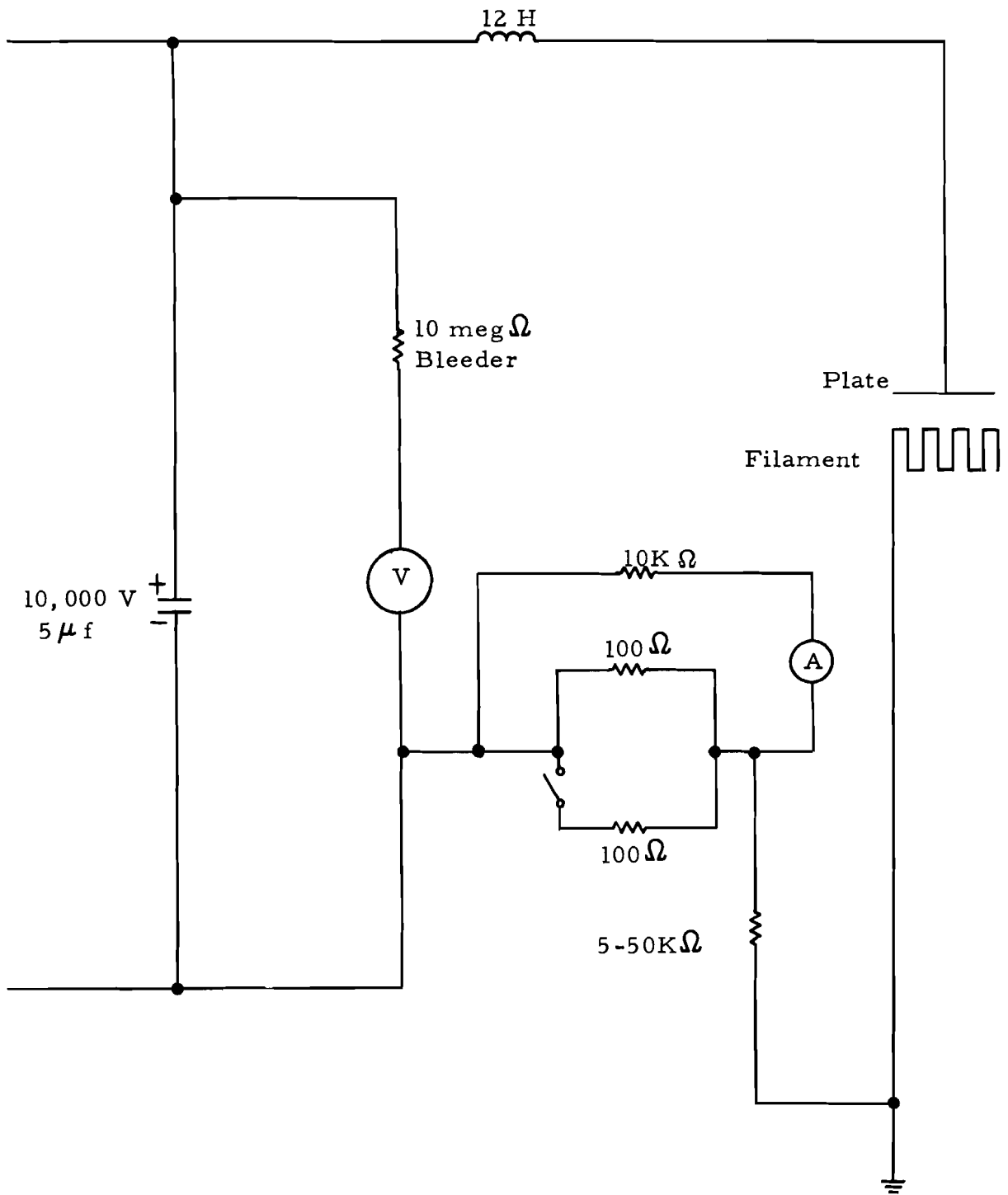
Figure 10. Schematic of Power Supply Meter Circuit.
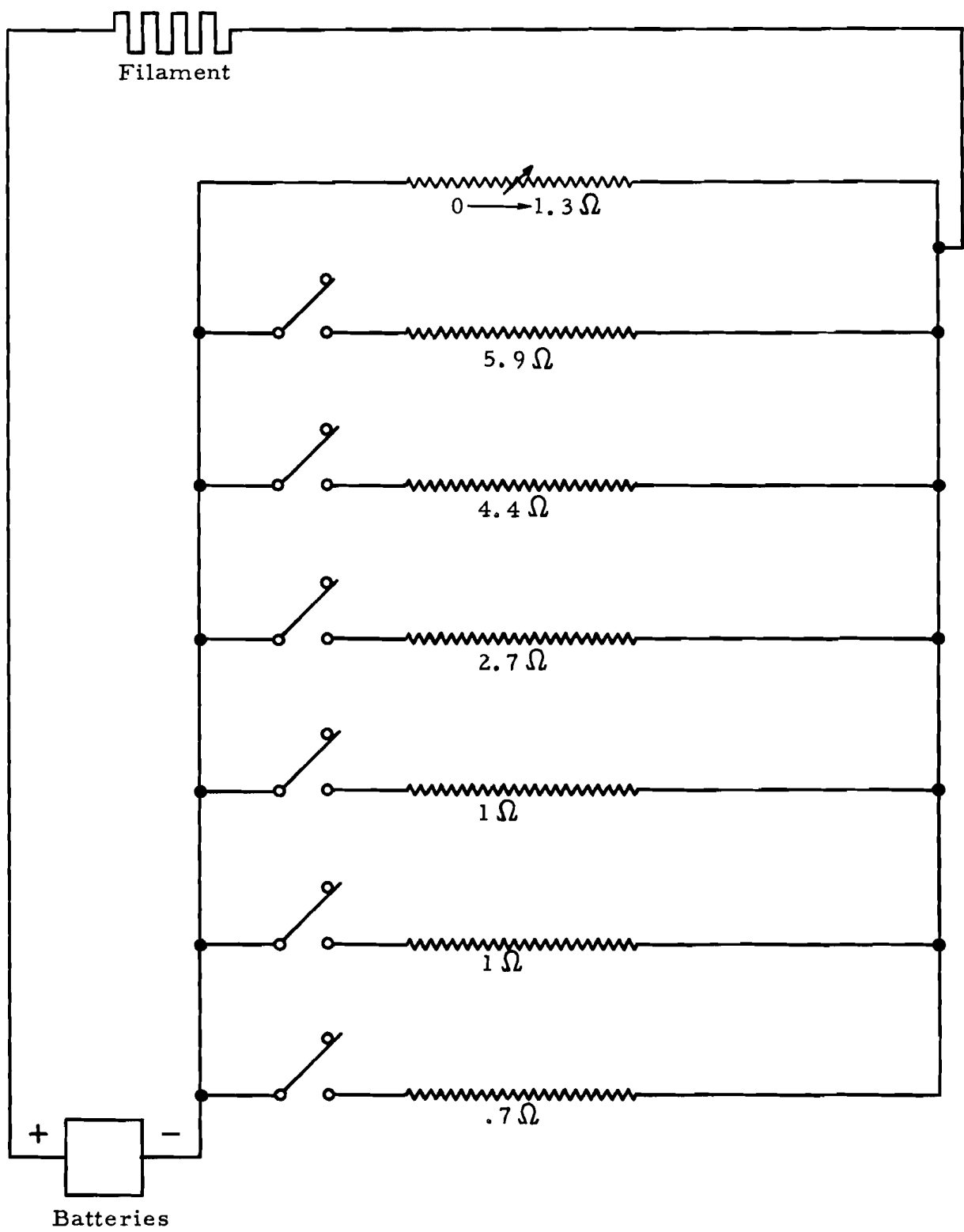
Figure 11. Schematic of Filament Power Supply.

operating time was gained because continuous operation of the batteries was only approximately 10 hours.

C. MEASURING EQUIPMENT

In the initial phases of this program phototubes were used as radiation detectors. The phototubes used were two RCA 6750 which, after calibration, were rigidly mounted on the viewing ports of the test chamber. The calibration method used was to sight a black body cavity whose temperature was measured with a thermocouple and to measure the potential drop across a one megohm resistor in series with the phototube. The black body used was an electrically heated laboratory furnace with the door replaced by insulating bricks having a viewing port cut through them. The phototubes were housed in metal cylinders with short lengths (about 1 inch long) of tubing attached at right angles to the cylinder to provide a viewing port and mounting bracket. Because of the lack of an optical system, the phototubes were sensitive to ambient light and difficult to position.

Further investigation into radiation detectors showed that by using a radiometer the infrared response was enhanced. Two radiometers were used to view the sample simultaneously. These instruments were calibrated before they were used.

Figure 12 shows the apparatus for calibrating the Barnes Engineering Co. model R-4D1 Radiometers. The instruments were

RADIOMETER HEAD   QUARTZ WINDOW   FURNACE   RADIOMETER HEAD

RADIOMETER AMPLIFIERS

POTENTIOMETER   GALVANOMETER
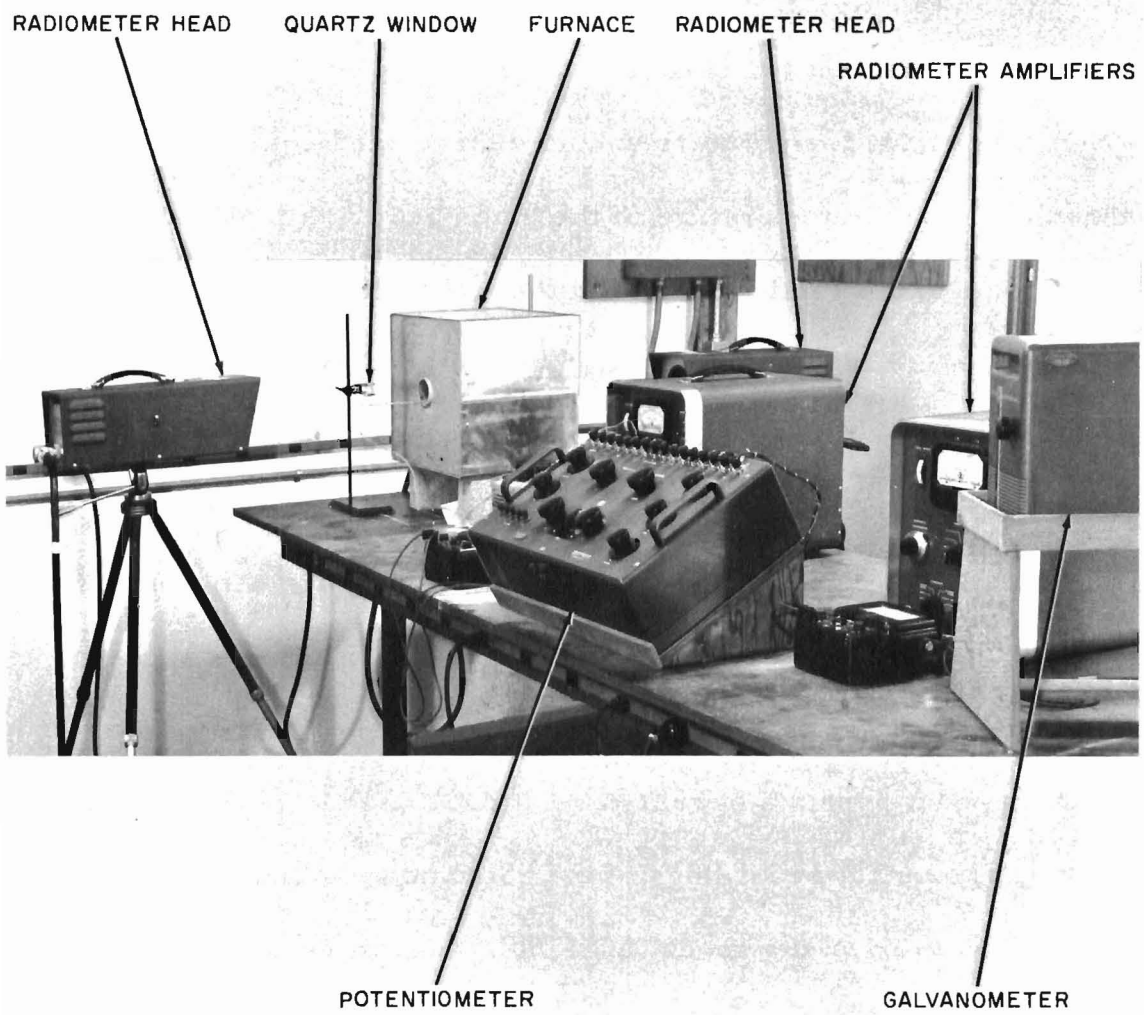
Figure 12. Experimental Setup for Calibrating Radiometers with Black Body.

27

sighted into a simple black body consisting of a small port in an electrically heated furnace. To obtain the temperature-rms voltage relationship required to plot the calibration curves, a series of observations were made at different temperatures. The black body was heated to a desired calibration temperature and held there until equilibrium was reached. Then the temperature of the black body was measured, using a thermocouple and potentiometer, and the rms voltage of the radiometers noted for sighting at the black body directly and also through a quartz window. In addition, the dc voltages at the output binding posts were recorded. Curves of temperature versus rms volts for sighting directly on the black body and also through a quartz window are shown in Figures 13 and 14. Curves were drawn showing the relationship between rms volts and dc output volts (Figures 15 and 16) in order that a power recorder could be used to obtain a written record.

The output recordings of the radiometers were obtained by using a Sanborn Recorder model 60-1300. In addition to measuring the temperature variation on the back face of the sample, the Tektronix dual-beam oscilloscope (type 502) provided the means of monitoring the power input to the sample by displaying the sinusoidal temperature variation being impressed on the front face of the sample. Polaroid pictures were taken of the dual beam which illustrate the temperature phase shift between the front and back faces of the sample. Figures 17 and 18 show the arrangement of the measuring instruments. Figure 19 is a block
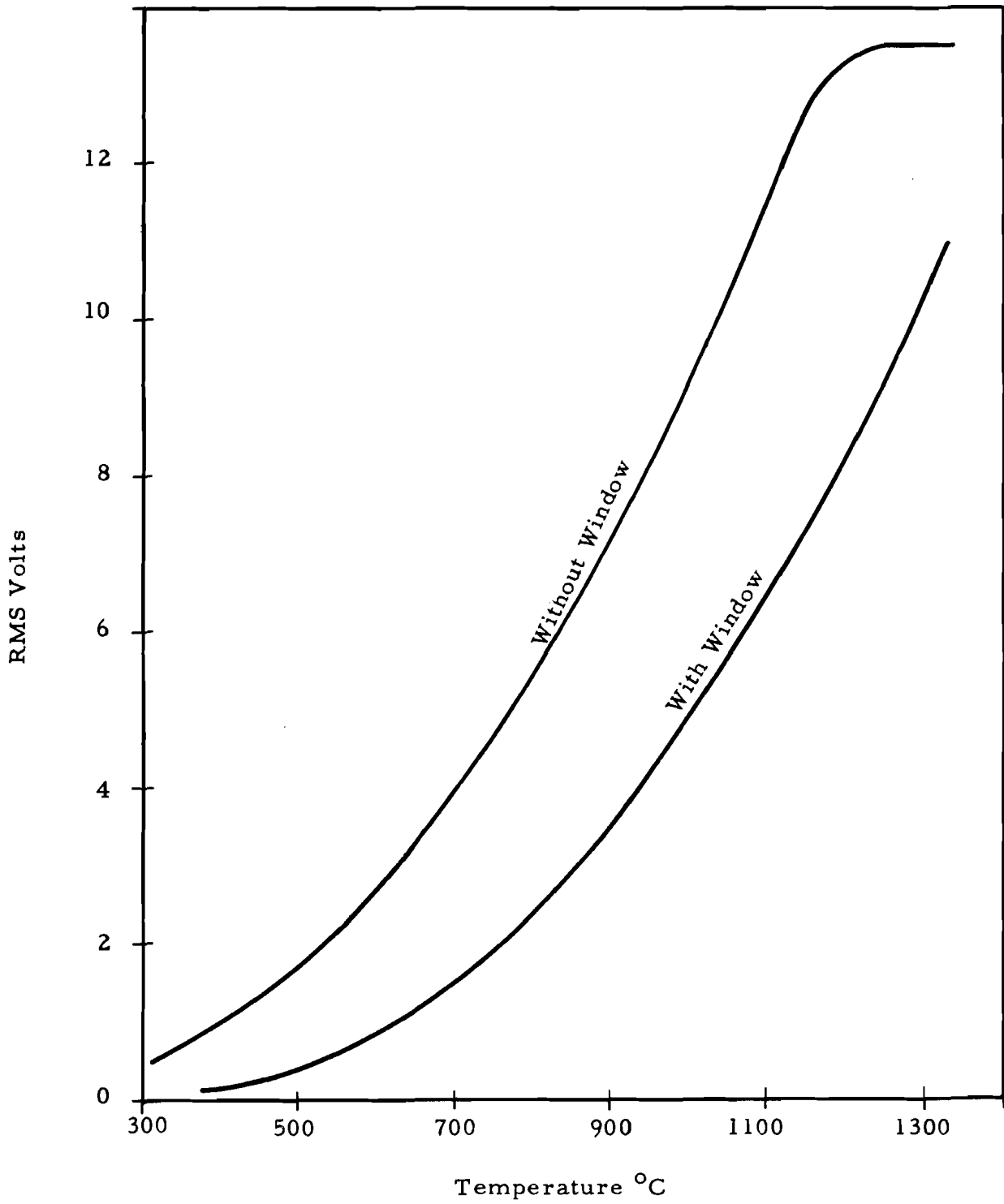
Figure 13. Calibration Curve of Radiometer No. 106.
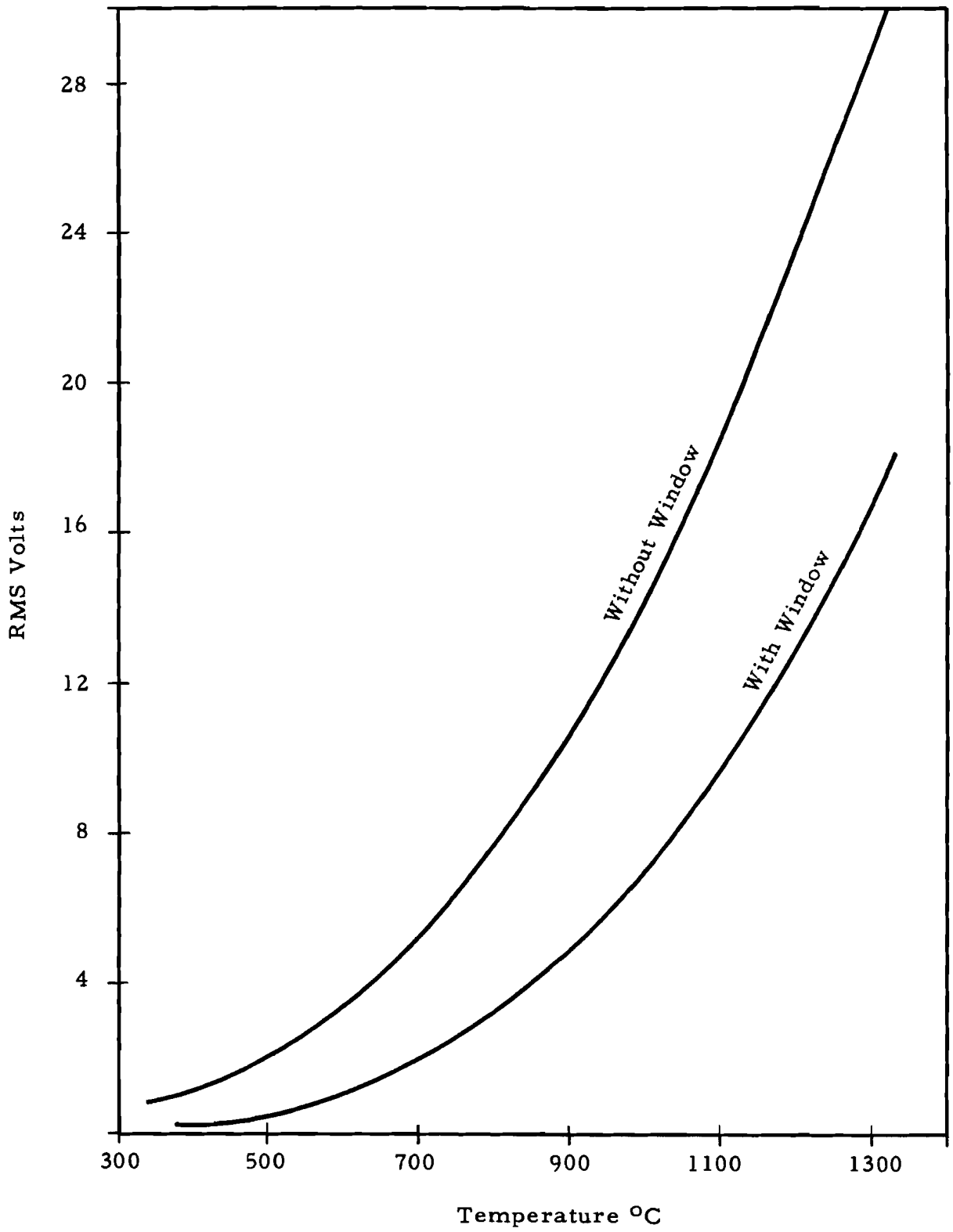
Figure 14. Calibration Curve of Radiometer No. 113.
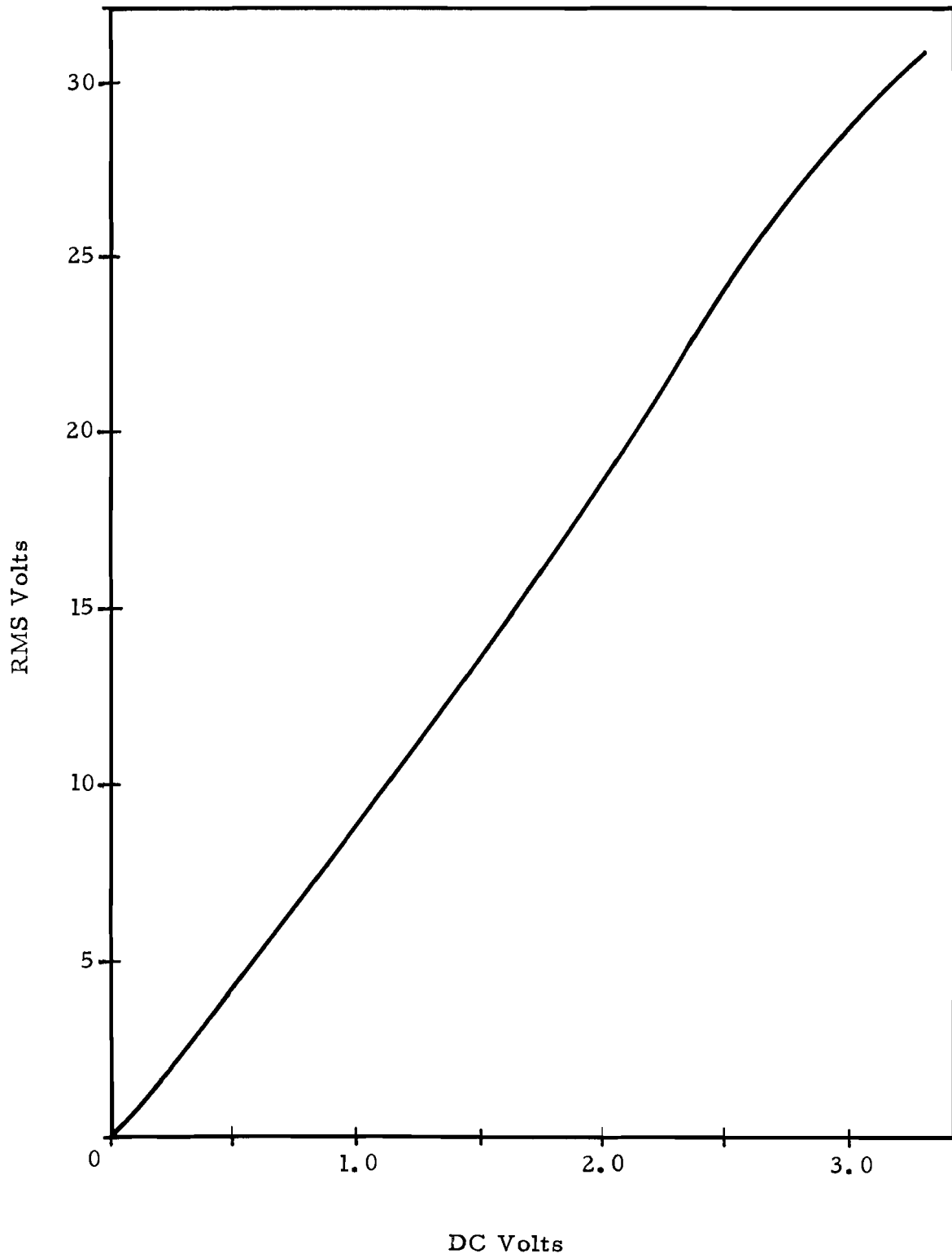
Figure 15. RMS Volts as a Function of DC Voltage Output for
Barnes Radiometer #113.
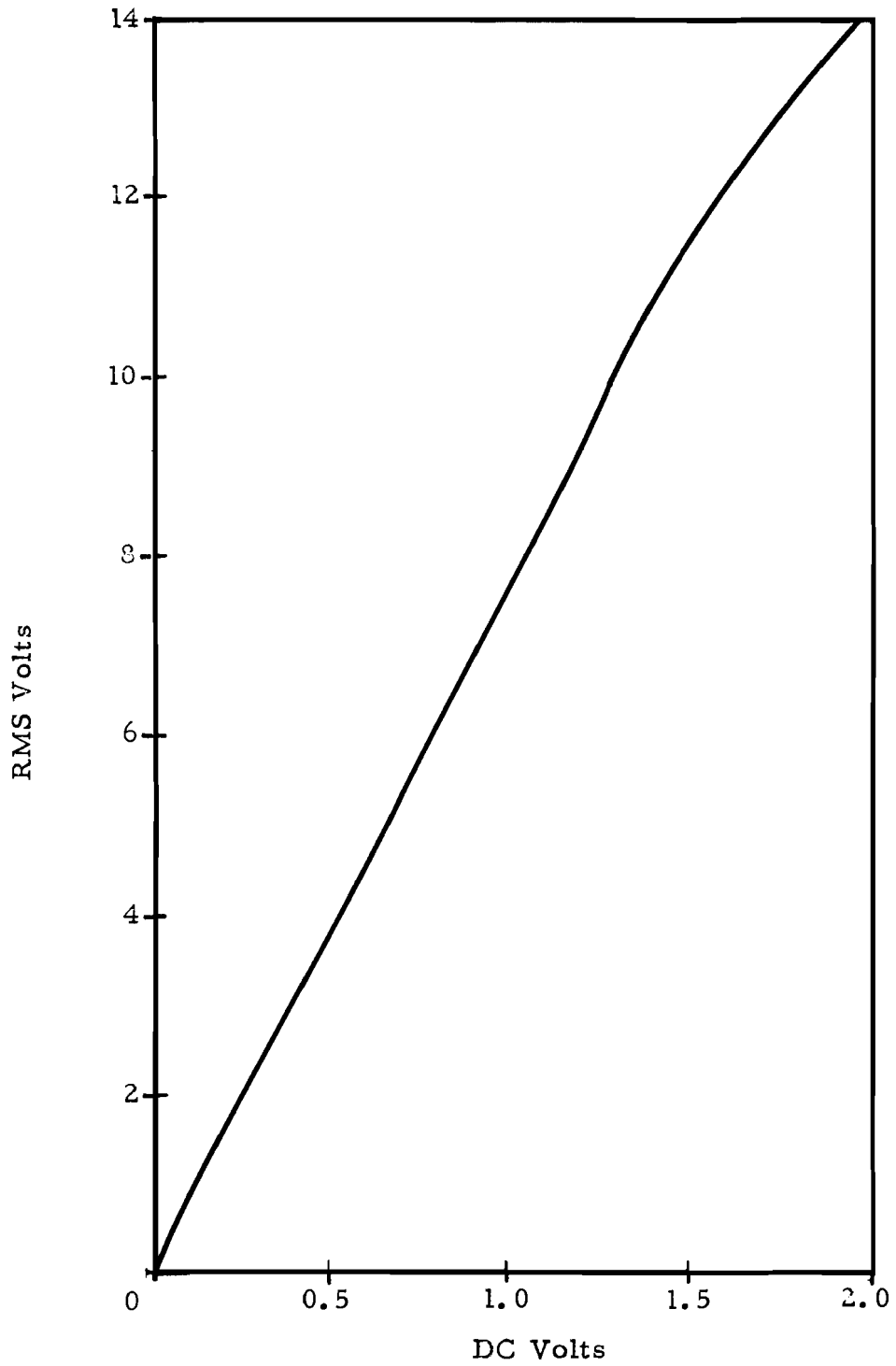
Figure 16. RMS Volts as a Function of DC Voltage Output for Barnes Radiometer #106.

VIEWING PORT   VACUUM GAGE METER   RADIOMETER AMPLIFIERS

POWER SUPPLY   OSCILLOSCOPE   AUDIO OSCILLATOR   RECORDER
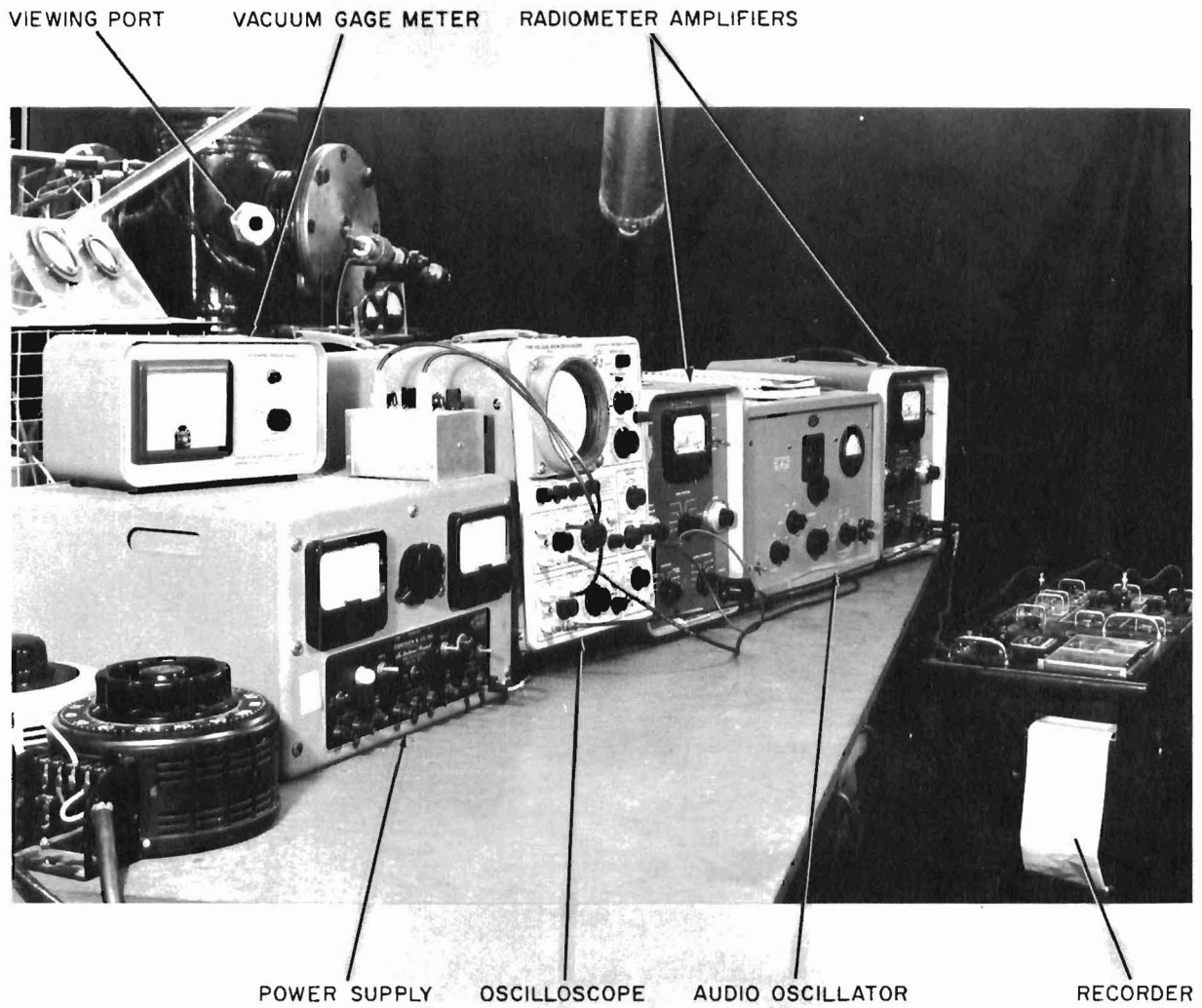
Figure 17. Measurement and Control Instrumentation, Non-Operating Setup.

33

PLATE METERS   TEST CHAMBER   OSCILLOSCOPE CAMERA

VACUUM GAGE METER

ACCELERATING POWER SUPPLY

HIGH VOLTAGE POWER SUPPLY   LINE VOLTAGE TO HIGH VOLTAGE POWER SUPPLY
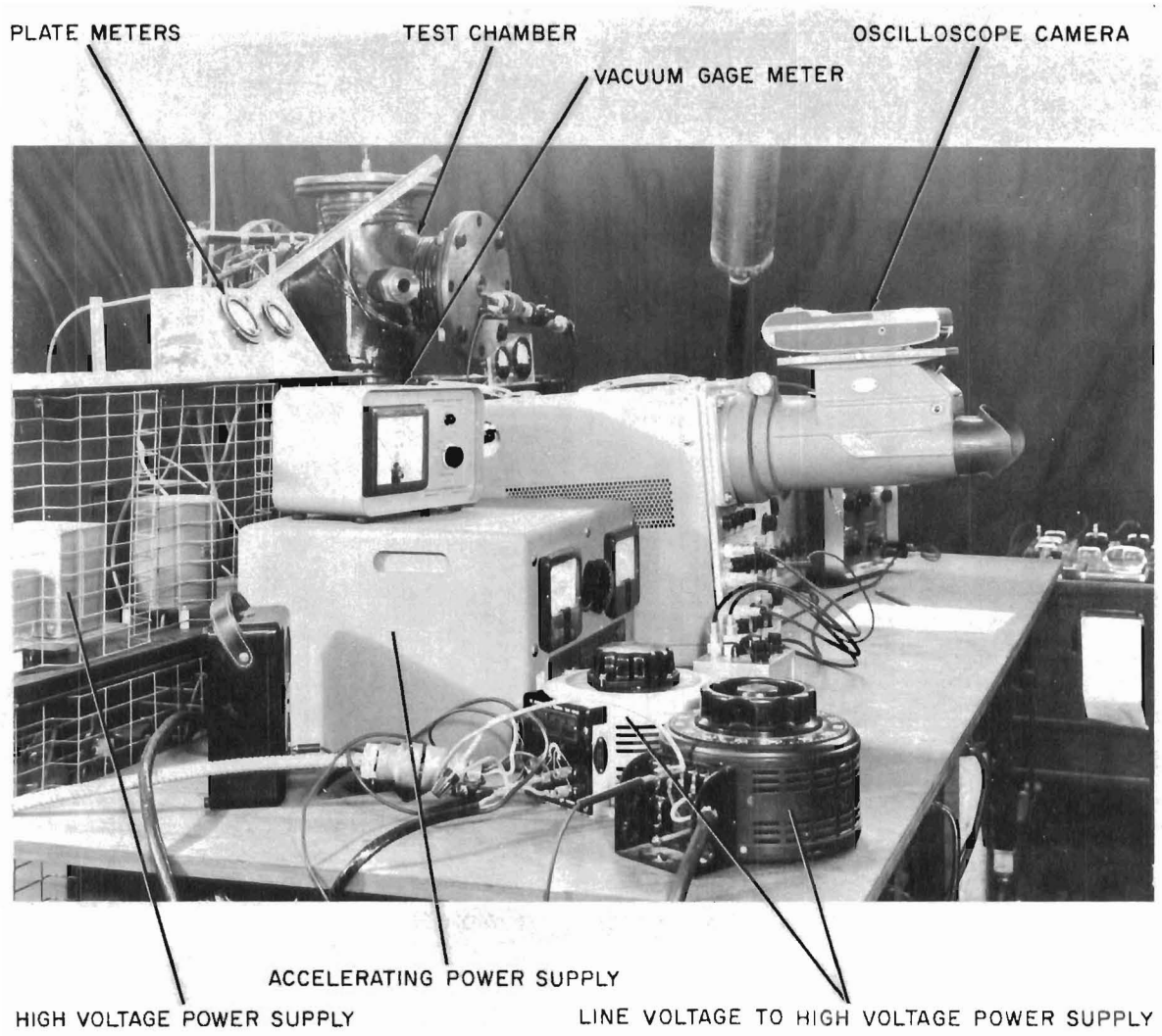
Figure 18. Measurement and Control Instrumentation, Operational
Setup with Camera in Place.

34
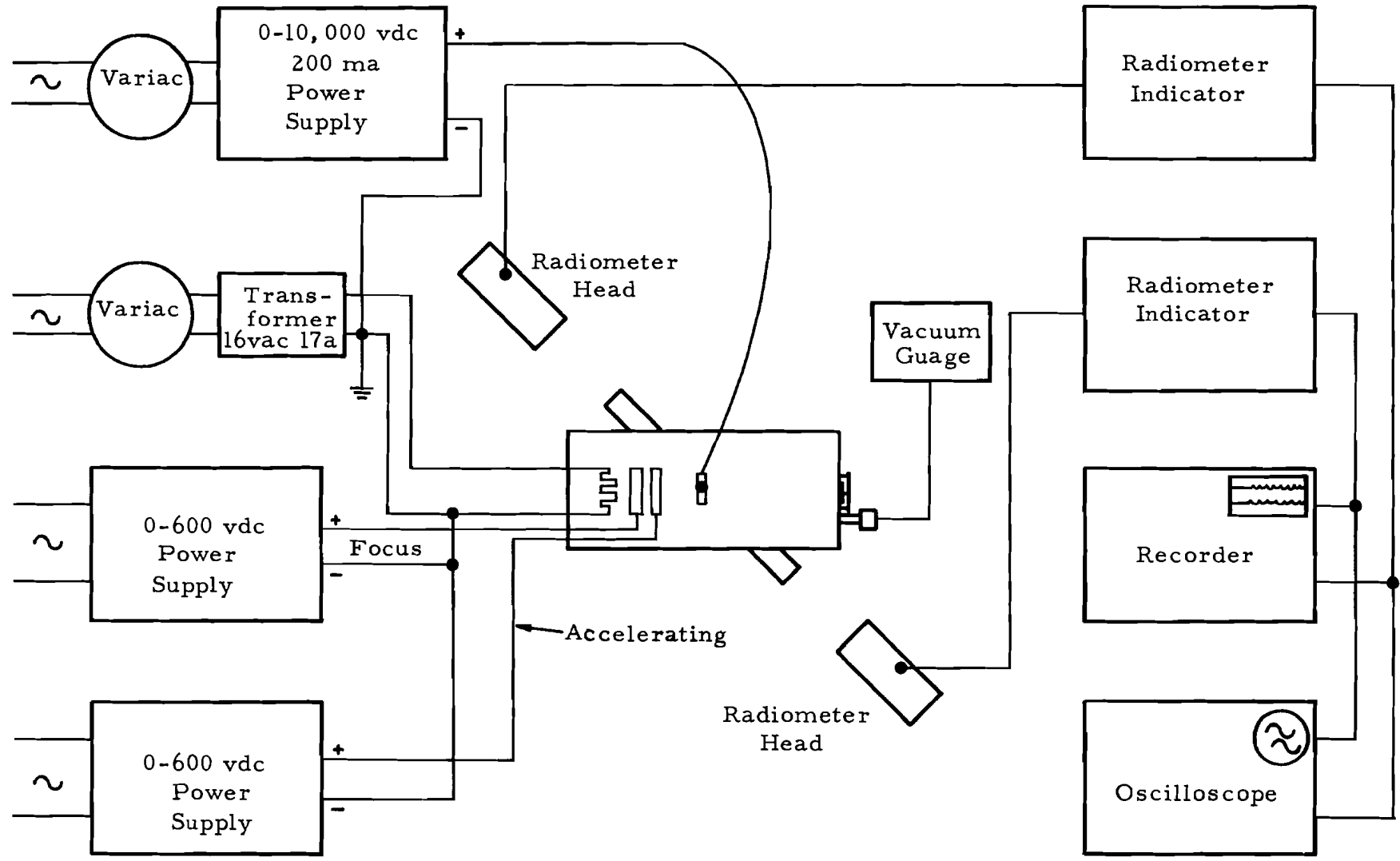
Figure 19. Block Diagram of Experimental Apparatus.

diagram of the over-all experimental arrangement, and Figure 20 shows

the arrangement in the laborabory.

D. MEASUREMENT OF THERMOPHYSICAL PROPERTIES

1. Sample Dimensions

The choice of sample shape was based on the need for a sample

with simple boundary conditions. The determination of sample thickness

was based on the need of obtaining sufficient shift in the temperature

wave peaks front to back. Hence, graphite having a conductivity greater

than Al_2O_3, the sample thickness was chosen as approximately twice the

latter.

2. Experimental Procedure

The sample to be measured was suspended by tungsten wire of

20 mils diameter and aligned so that the area vector of the rear face was

perpendicular to the face of the rear viewing port (Figures 2 and 3). The

chamber was then evacuated to an operational vacuum of 10^{-5} mm Hg and

the radiometers were rough focused by sighting on the sample faces.

Slow heating was then commenced by control of the driving and focusing

potentials until an approximation of the desired steady nonperiodic tem-

perature was reached. At this point the radiometers were fine-adjusted

by refocusing for maximum output on their respective amplifiers. After

refocusing, the sample temperature was adjusted to the value desired as

RADIOMETER HEAD   TEST CHAMBER   OSCILLOSCOPE CAMERA

VACUUM GAGE METER   RADIOMETER HEAD

VACUUM PUMP

FOCUSING RING POWER SUPPLY   HIGH VOLTAGE POWER SUPPLY
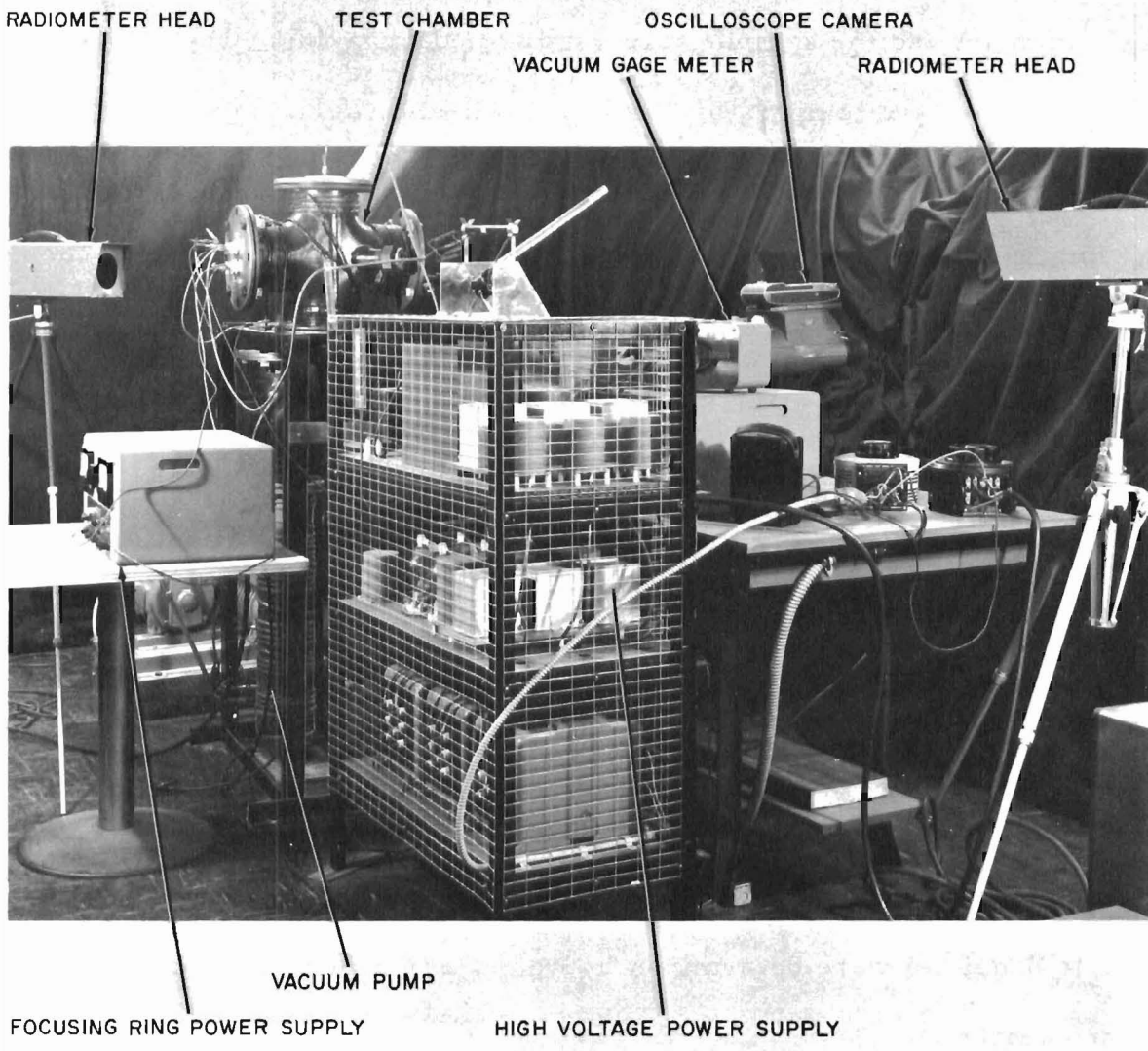
Figure 20. Over-all View Showing Position of Radiometer Heads.

37

indicated by the radiometer outputs. The oscilloscope and power recorder were adjusted for calibration and null reading. From this point the equipment and the sample were ready for data taking. The imposition of a sine wave temperature was maintained by scribing an exact sine wave of proper amplitude on the face of the oscilloscope. By manually varying the power input the front face radiometer signal imposed on the oscilloscope could be forced to follow the sine wave pattern. The frequency of the temperature wave was then determined by the time per cm calibration on the scope. The back face temperature as indicated by the radiometer was allowed to follow its own wave form. The resulting peak to peak lag in the two waves was then used to determine the sample diffusivity as given in the data analysis. The sample was then heated in a controlled temperature furnace with a thermocouple to determine true sample temperature. By measuring the black body temperature with the radiometer a calculation of emissivity can be made from equation 29. Sample densities were determined by weight and volume measurements before heating.

3. Sample Deterioration

In the early heating trials, various methods of beam focusing were tried without success. The result was a pencil-like beam with a high concentration of electrons $/cm^2$ with a resulting sputtering due to secondary electron emission and scoring of the sample surface. The final focusing method used was similar to the electrostatic focusing

rings used in the electron gun of a cathode ray tube. The principle employed was that when an electron beam passes through a retarding potential it slows down and tends to disperse, and when accelerated it converges. Since it was only necessary to spread the beam, only the retarding potential field was used. With this innovation the effects of sputtering were made negligible since the beam could now be spread evenly over the face of the sample to obtain uniform heating. This also made it possible to increase the electron densities and decrease the individual mean velocity so as to impart the same energy with less occurrence of sputtering. It was easy to determine when sputtering was negligible, because its occurrence was sufficient to prove disastrous to the vacuum conditions of the chamber, and usually resulted in a blown fuse.

IV. DATA ANALYSIS

A. CALCULATION OF α

The expression for the phase angle ϕ as given in the theory is

$$\phi = \tan^{-1}\left[\frac{\tanh \beta\ell \tan \beta\ell - (K/\beta\ell)[\tanh \beta\ell - \tan \beta\ell]}{1 + (K/\beta\ell)[\tanh \beta\ell + \tan \beta\ell]}\right] \text{ where } K = \ell h/2k.$$

Measurements of ϕ were made for Al_2O_3 at $1290^{\circ}K$ and $1400^{\circ}K$, and for

graphite at $1189^{\circ}K$. Recalling that the value of K (equal to 0.147) re-

lated to the measurement on Al_2O_3 at $1400^{\circ}K$ was the largest encoun-

tered, the corresponding curve has the nature of a lower bound. Hence,

curves associated with smaller values of K will lie between that of equa-

tion 27 and that of equation 28 (for which K = 0). Tables I and II give

values of α for Al_2O_3 and graphite, respectively, for the two extreme

cases K = 0 and K = 0.147. Most measurements were made for $\beta\ell < 1$

radian. In this region the value of α derived from the former curve is

too high, whereas the opposite is true with respect to the latter curve.

Since the two curves of equations 27 and 28 approach each other as $\beta\ell$

increases, it is clear that experiments designed for larger values of $\beta\ell$

are most easily interpreted. This fact is verified by the values of α

taken from the literature[5]. For example, these other sources list, for

Al_2O_3, α = 0.011 at $1290^{\circ}K$. It may be noted in Tables I and II that the

best agreement occurs at the smallest values of τ (i.e., at the largest

frequencies).

TABLE I

Thermal Diffusivity of P. C. Al_2O_3

Run No.	Tas(°K)	l(cm)	τ(sec)	t(sec)	φ(rad)	K = 0		K = 0.147	
						βl(rad)	$\alpha(cm^2 sec^{-1})$	βl(rad)	$\alpha(cm^2 sec^{-1})$
1	1289	0.255	50	4.5	0.565	0.774	0.0068	0.835	0.0067
2	1289	"	50	5.0	0.628	0.82	0.0064	0.888	0.0052
3	1292	"	50	4.5	0.565	0.774	0.0068	0.835	0.0067
4	1408	"	50	5.0	0.628	0.82	0.0064	0.888	0.0052
5	1409	"	50	4.2	0.527	0.744	0.0073	0.802	0.0064
6	1397	"	50	5.0	0.628	0.82	0.0064	0.888	0.0052
7	1397	"	50	5.0	0.628	0.82	0.0064	0.888	0.0052
8	1397	"	20	3.3	1.03	0.908	0.0124	1.03	0.0096
9	1397	"	20	3.3	1.03	0.908	0.0124	1.03	0.0096

41

TABLE II

Thermal Diffusivity of Graphite

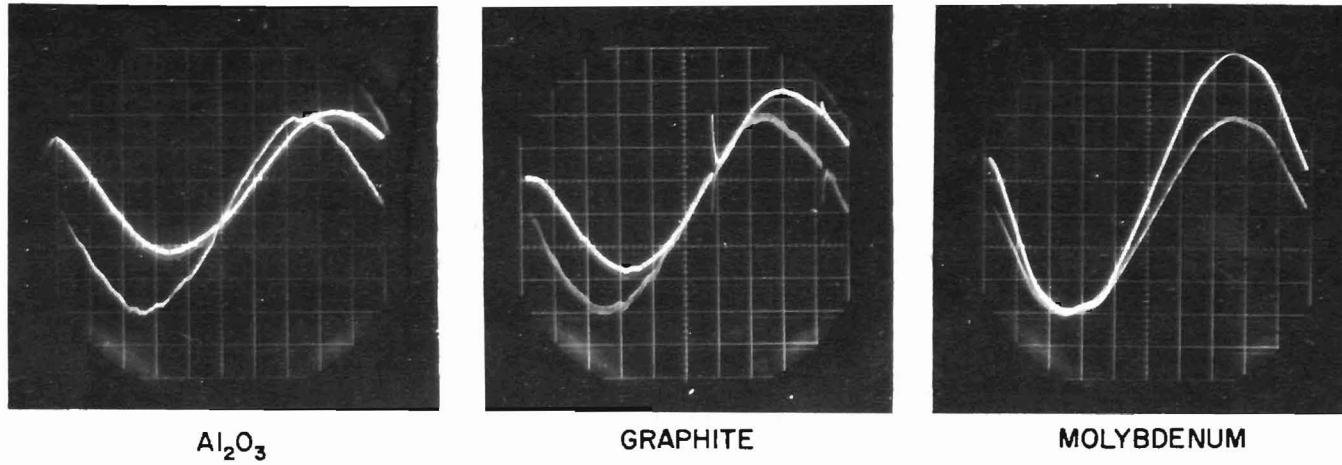| Run No.	$T_{as}(^\circ K)$	l(cm)	τ(sec)	t(sec)	ϕ(rad)	K = 0		K = 0.147	
						βl(rad)	α(cm^{2}sec^{-1})	βl(rad)	α(cm^{2}sec^{-1})
1	1193	0.5	50	2.6	0.326	0.576	0.0473	0.622	0.0407
2	1185	"	50	2.62	0.329	0.58	0.0468	0.625	0.0403
3	1185	"	20	1.65	0.518	0.737	0.0723	0.795	0.0622
4	1194	"	10	1.15	0.722	0.89	0.0992	0.962	0.0854

Figure 21. Oscilloscope Photographs of Temperature Wave Phase Shift in Al_2O_3, Mo and Carbon.
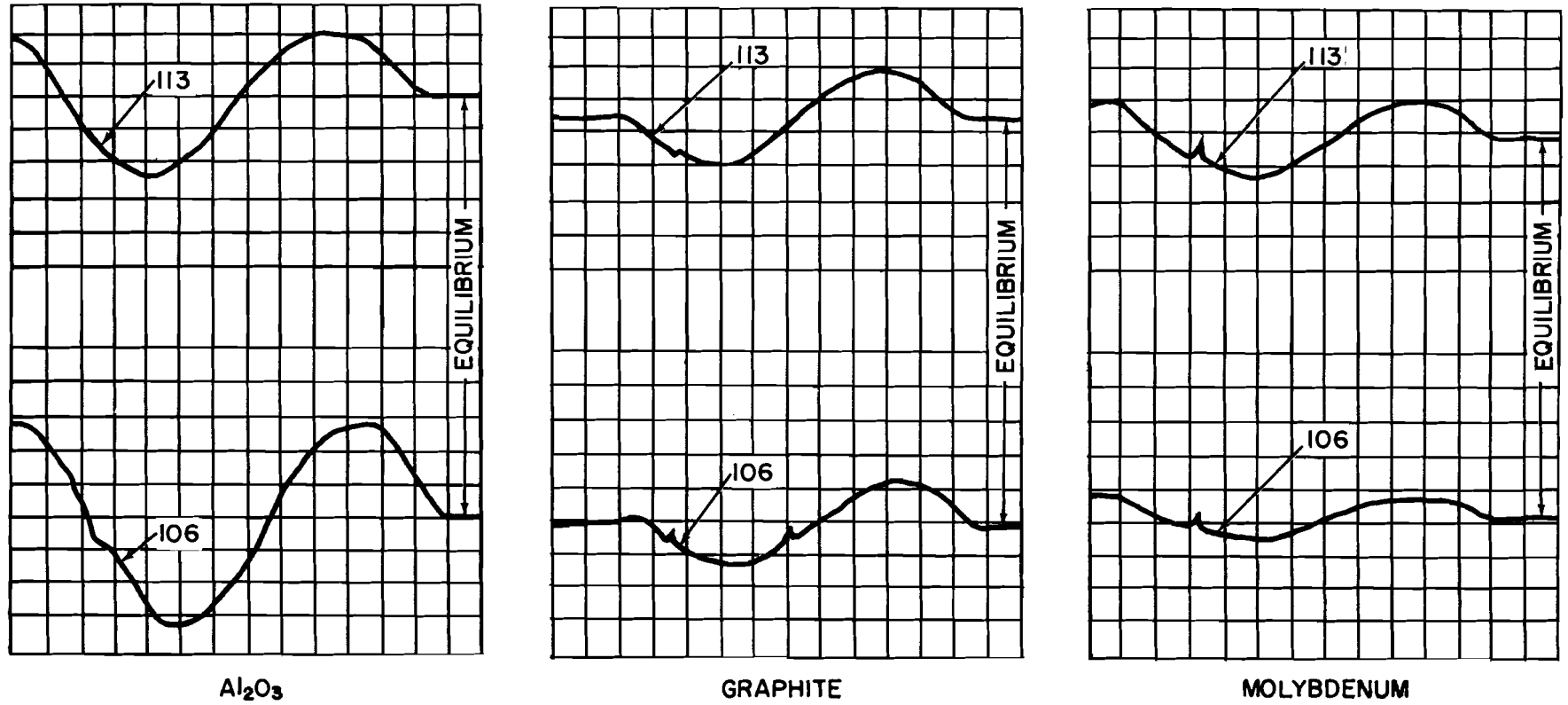
Figure 22. Sanborn Recorded Traces of Power Output of Radiometers 106 and 113.

B. MEASUREMENT OF EMISSIVITY

The total normal emissivity, ϵ, can be calculated from equation 29 by a measurement of power output of a black body and of the sample, both at the same temperature. In the process of electron bombardment it is necessary to conduct away the plate charge as it accumulates. Hence, it is necessary to coat the surface of a nonconductor with a thin graphite film. This coating introduces an error in the measured temperature gradient (front to back). By making independent measurements of the emissivities of both the clean and coated surfaces it is possible to correct the error in the temperature gradient. Tables III, IV, and V give values of total normal emissivity for polycrystalline Al_2O_3 for the clean and coated surfaces, and for graphite. Figures 23 and 24, and 25 are curves of emissivity versus degrees Kelvin for the three samples under consideration. Figure 26 shows a curve of rms output of the radiometer versus temperature in degrees Kelvin for the measurement of emissivity. This curve is calibrated against a black body, and hence is read in equivalent black body temperature. Since both readings of black body and sample are made at the same temperature, the total normal emissivity is the ratio of the power radiated from the black body to the power radiated from the sample or

$$\epsilon_s = \frac{P_s}{P_B} ,$$

where P_s is the power radiated from the sample and P_B is the power radiated from the black body, when the temperatures are the same.

TABLE III

Total Normal Emissivity of P. C. Al_2O_3 (clean)

Furnace $^{\circ}K$	rms volts black body	T_b $^{\circ}K$	rms volts Al_2O_3	T_s $^{\circ}K$	Power (w/cm^2) black body	Power (w/cm^2) Sample	ϵ
1043	5.0	1047	2.7	870	6.84	3.28	.480
1045	5.0	1047	2.8	879	6.84	3.40	.497
							$\overline{\epsilon}$ = .489
1168	7.01	1167	4.6	1020	10.55	6.15	.583
1171	7.30	1182	4.6	1020	11.08	6.15	.555
							$\overline{\epsilon}$ = .569
1482	12.8	1431	12.3	1404	23.8	22.05	.926
1481	12.8	1431	12.3	1404	23.8	22.05	.926
1481	12.8	1431	12.4	1408	23.8	22.35	.939
1482	12.8	1431	12.4	1408	23.8	22.35	.939
1482	12.8	1431	12.5	1414	23.8	22.65	.952
							$\overline{\epsilon}$ = .936

TABLE IV

Total Normal Emissivity of P. C. Al_2O_3 (Graphite Coated)

Furnace $^{\circ}K$	rms volts black body	T_b $^{\circ}K$	rms volts Al_2O_3	T_s $^{\circ}K$	Power (w/cm^2) black body	Power (w/cm^2) Sample	ϵ
1047	5.05	1050	4.1	984	6.91	5.31	.768
1049	5.05	1050	4.1	984	6.91	5.31	.768
							$\bar{\epsilon}$ = .768
1175	7.38	1187	6.6	1143	11.28	9.69	.860
1176	7.38	1187	6.6	1143	11.28	9.69	.860
							$\bar{\epsilon}$ = .860
1482	12.9	1439	12.5	1414	24.35	22.65	.930
1483	12.9	1439	12.6	1419	24.35	22.97	.944
1481	12.9	1439	12.5	1414	24.35	22.65	.930
							$\bar{\epsilon}$ = .935

47

TABLE V

Total Normal Emissivity of Graphite Cylinder

| Furnace ^{o}K	rms volts black body	T_b ^{o}K	rms volts Graphite	T_s ^{o}K	Power (w/cm^2) black body	Power (w/cm^2) Sample	ϵ
1050	5.13	1055	4.8	1034	7.05	6.50	.922
1052	5.15	1057	4.8	1034	7.09	6.50	.917
							$\bar{\epsilon}$ = .920
1177	7.41	1188.5	7.0	1166	11.33	10.50	.925
1179	7.43	1190	7.1	1170	11.39	10.65	.935
							$\bar{\epsilon}$ = .930
1481	12.9	1439	12.7	1425	24.35	23.4	.961
1481	12.9	1439	12.7	1425	24.35	23.4	.961
1482	12.9	1439	12.8	1431	24.35	23.8	.978
1482	12.9	1439	12.7	1425	24.35	23.4	.961
							$\bar{\epsilon}$ = .965

58
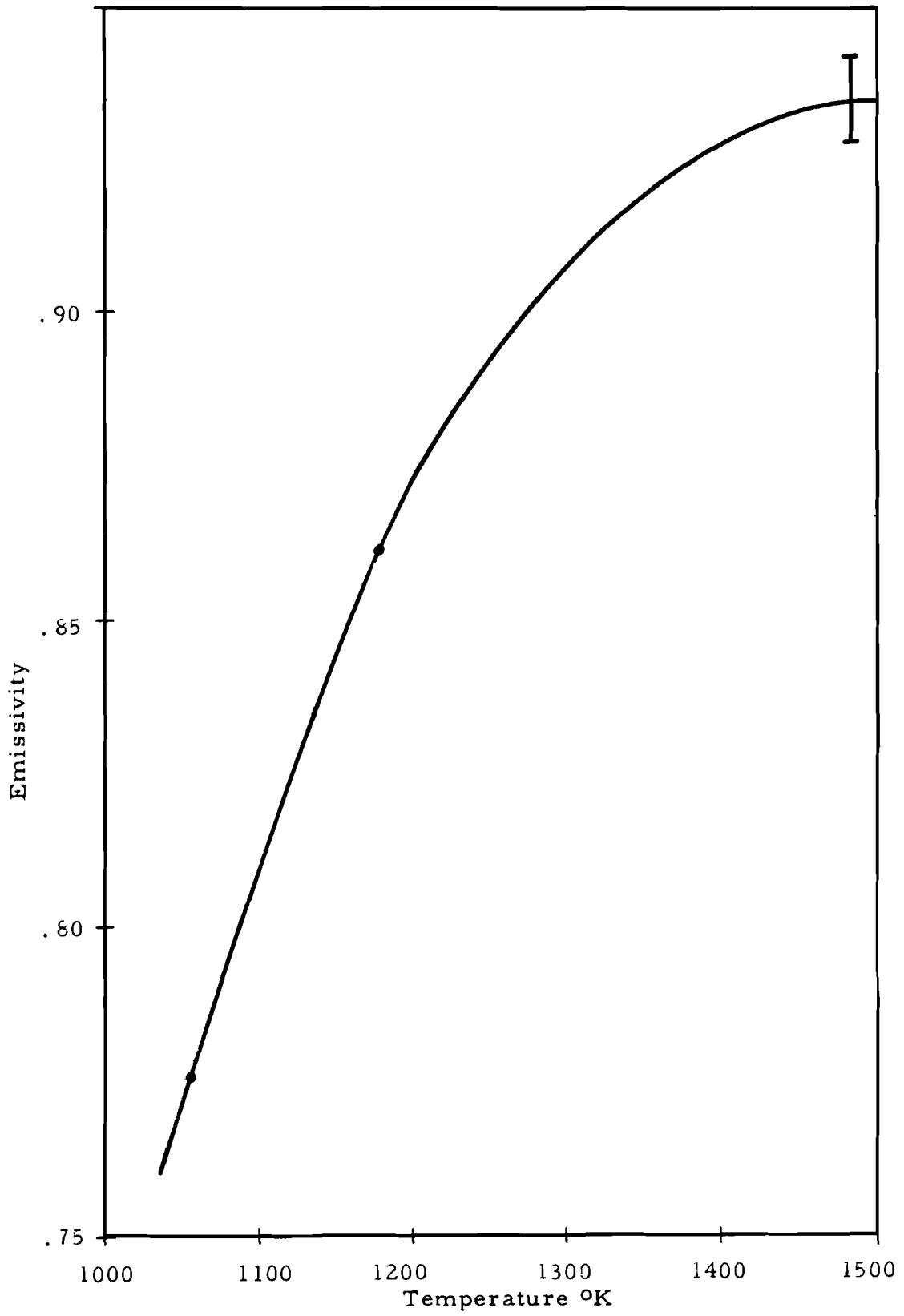
Figure 23. Graph of Temperature vs Emissivity for Dag Coated P.C. Al_2O_3.
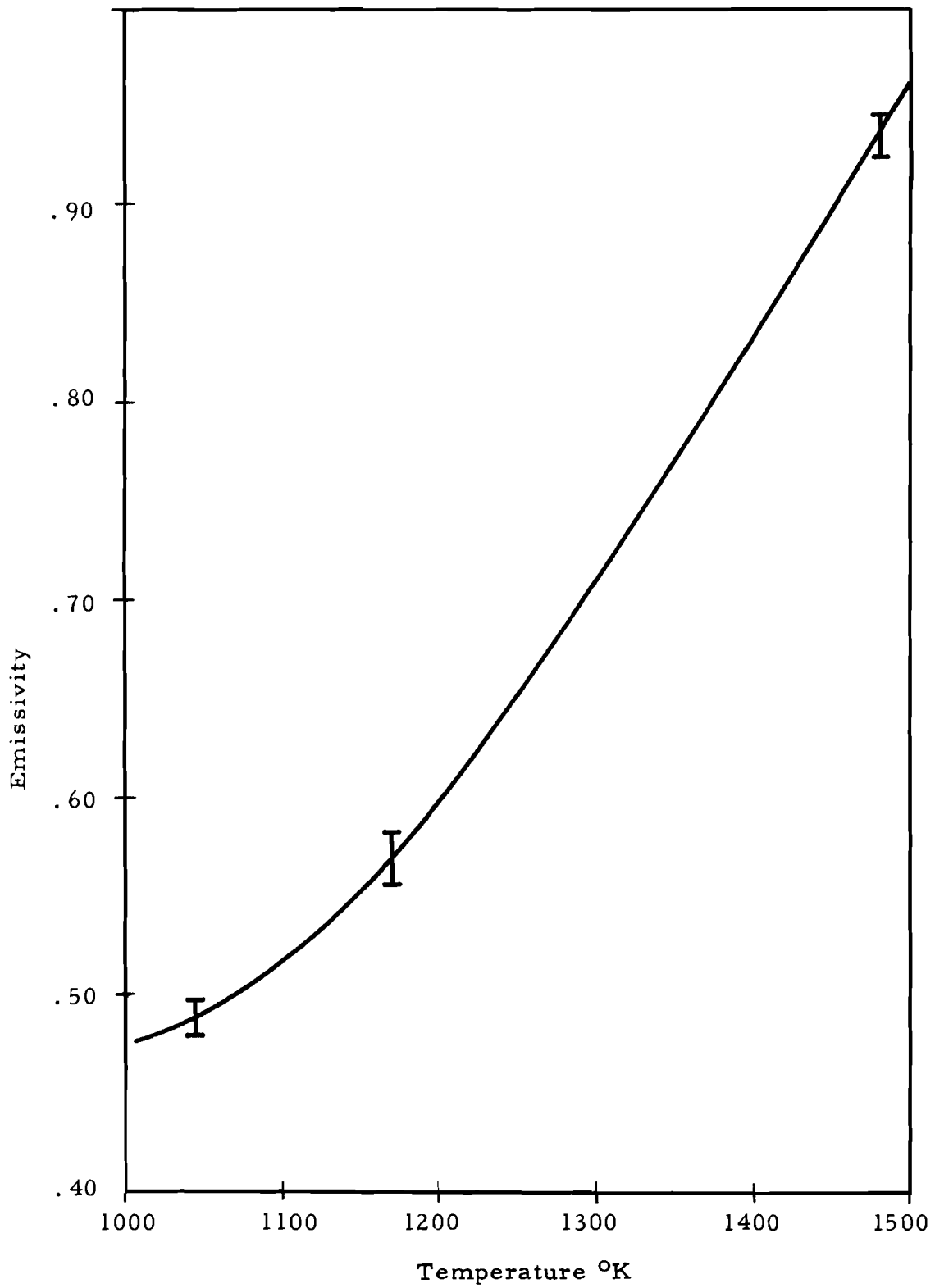
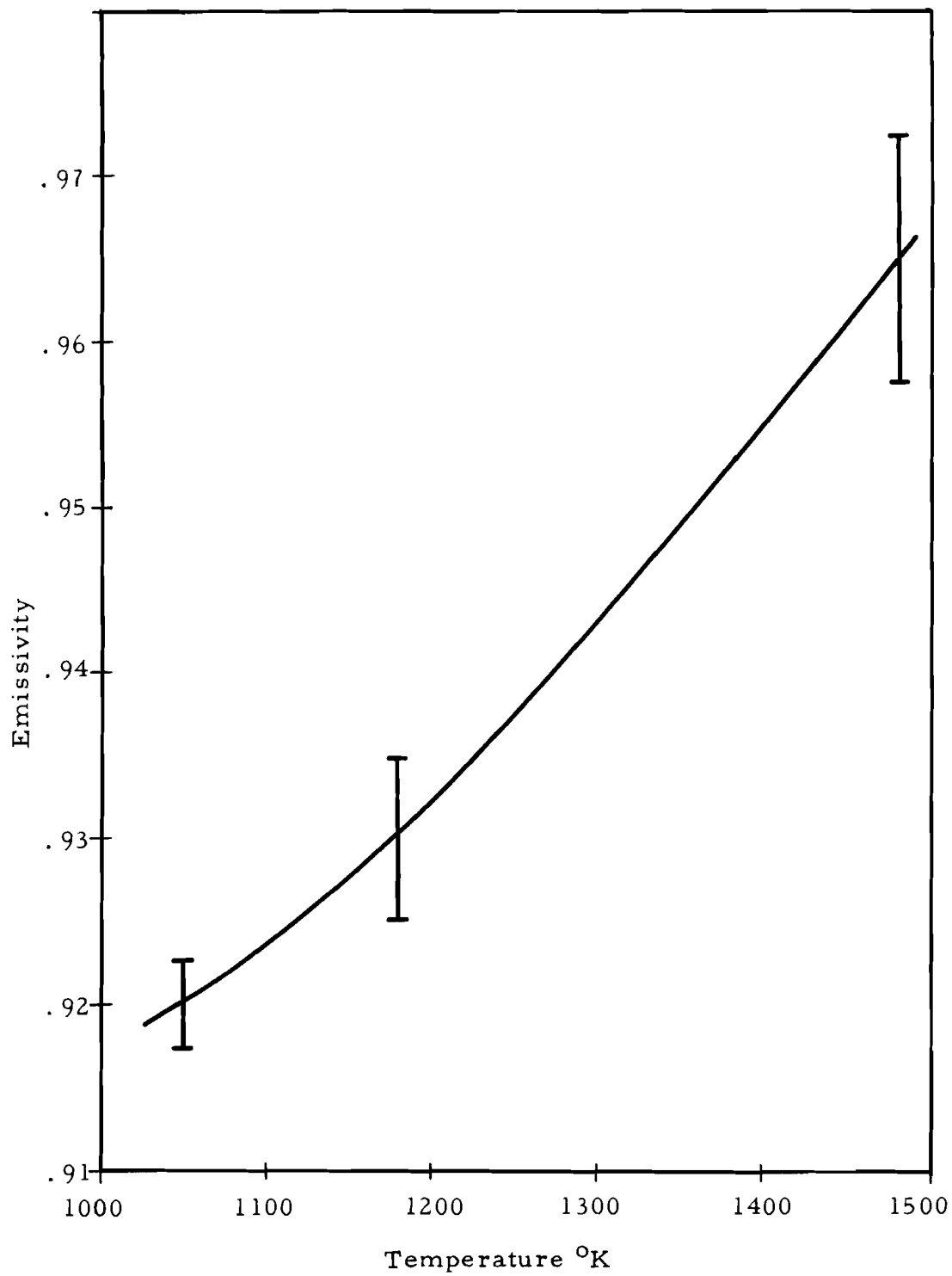Figure 24. Graph of Temperature vs Emissivity for Clean P. C. Al₂O₃.

Figure 25. Graph of Temperature vs Emissivity for Graphite.

51
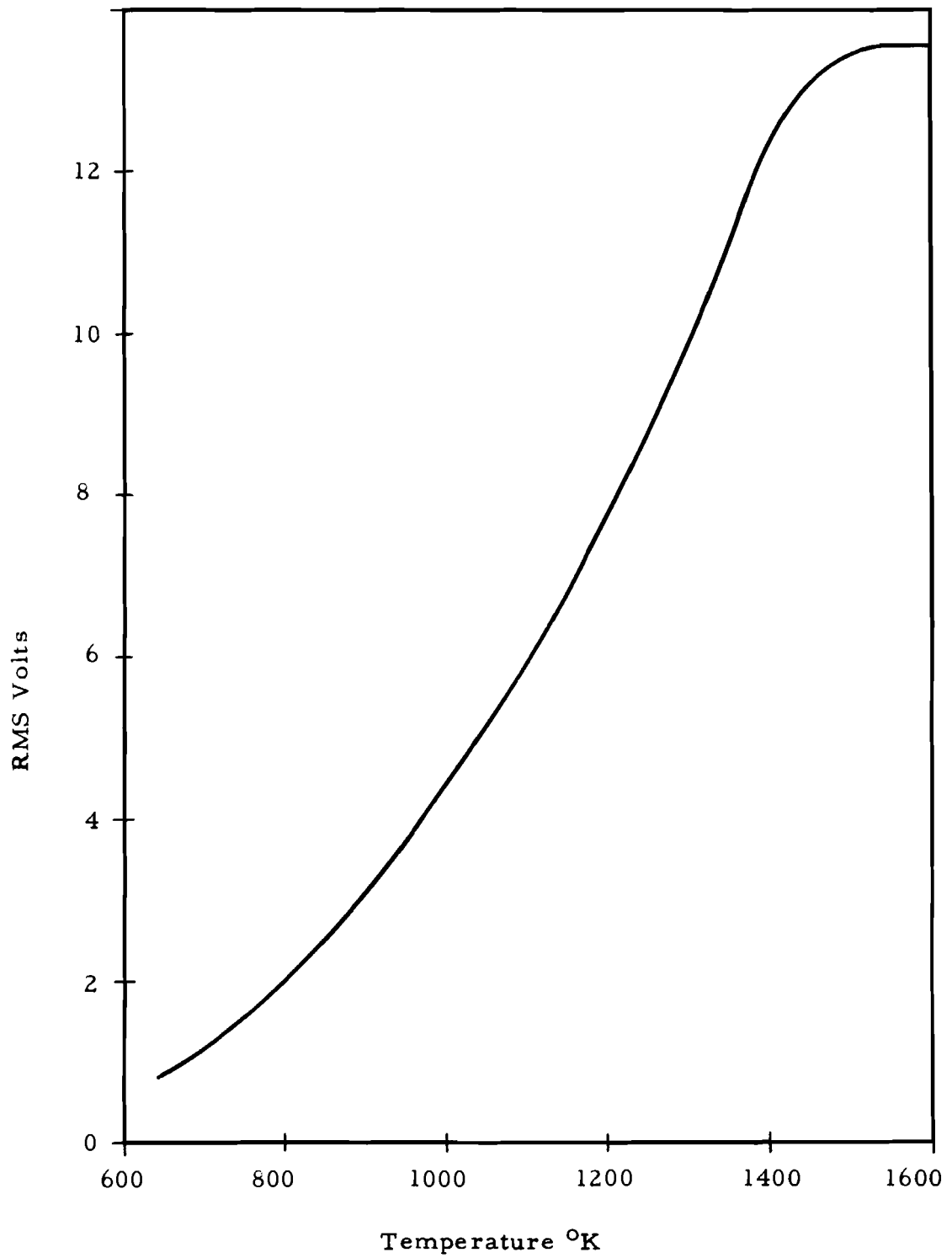
Figure 26. Graph of Temperature vs RMS Volts for Radiometer Head No. 106.

The average values of emissivity, $\bar{\epsilon}$, are given in the tables under the column to which they apply for each temperature. For the three temperatures the standard deviations are: Al_2O_3 (clean), $\sigma = 0.0085$, 0.014, and 0.01. The percentage standard deviations are 1.7%, 2.46%, and 1.06%. For the emissivity of the coated sample the standard deviation is $\sigma = 0.007$ for the highest temperature with a percentage deviation of 0.75%. The standard deviations for graphite are: $\sigma = 0.0038$, 0.005, and 0.0074. The respective percentage deviations are 0.4%, 0.5%, and 0.76%.

C. CALCULATION OF k

With values of α and ϵ determined for the materials, values of conductivity, k, have been calculated from equation 30 and are tabulated in Tables VI and VII for polycrystalline Al_2O_3 and for Graphite.

Since there are inaccuracies in both front and back temperature measurements due to suspected error in the radiometer calibration, average values of conductivity have been calculated from Tables VI and VII for average front (T_{af}) and back (T_{ab}) face temperatures and average sample temperature (T_{as}). Note again that the reason for two values of emissivity in Table VI, front and back, is the thin conducting graphite coat on one face. For a conductor such as graphite this was unnecessary and only one value of ϵ is given. For Al_2O_3 the standard deviation at $1290^\circ K$ is $\sigma = 0.136 \times 10^{-2}$ and at $1400^\circ K$ $\sigma = 0.406 \times 10^{-2}$ with

TABLE VI

Thermal Conductivity of P. C. Al_2O_3

Run No.	T_{af} Sample Temperature Front(°K)	T_{ab} Back(°K)	ΔT °K	Radiated Power (Back(cal/sec.)	Emissivity Front	Back	Thermal Conductivity (cal sec^{-1} cm^{-1} °C^{-1})
1	1337	1299	38	2.020	0.906	0.522	1.356×10^{-2}
2	1357	1310	47	2.115	0.912	0.530	1.151×10^{-2}
3	1300	1268	32	1.750	0.894	0.502	1.394×10^{-2}
4	1308	1271	37	1.895	0.892	0.516	1.307
5	1429	1386	43	3.130	0.928	0.622	1.854
6	1429	1389	40	3.170	0.928	0.626	2.020
7	1289	1263	26	1.710	0.890	0.499	1.615

T_{as} = 1290°K: $\bar{k}$ = 0.01418

T_{as} = 1400°K: $\bar{k}$ = 0.01675

TABLE VII

Thermal Conductivity of Graphite

Run No.	T_{af} Sample Temperature Front(°K)	T_{ab} Temperature Back(°K)	*ΔT- 17ΔT °K	Radiated Power Back(cal/sec.)	Emissivity	Thermal Conductivity (cal. sec^{-1} cm^{-1} °C^{-1})
1	1206	1180	21.5	2.631	0.932	0.0614
2 3	1193	1177	13.0	2.620	0.932	0.1008
3	1193	1177	13.0	2.620	0.932	0.1008
4	1208	1180	23.0	2.631	0.932	0.0574
5	1198	1180	14.9	2.631	0.932	0.0866
6	1198	1180	14.9	2.631	0.932	0.0866

$\overline{k}$ = 0.0829 T_{af} = 1199°K T_{ab} = 1179°K T_{as} = 1189°K

* (ΔT - .17ΔT) is the measured temperature difference minus the calculated temperature loss due to radiative heat transfer from the sides of the sample. This is necessary because of the thickness of the sample used.

average standard deviations of $\sigma_{av} = 0.068 \times 10^{-2}$ and $\sigma_{av} = 0.237 \times 10^{-2}$, respectively. The percentage of standard deviation is 9.6% and 24.2%, respectively. For graphite $\sigma = 1.88 \times 10^{-2}$ with an average standar standard deviation of $\sigma_{av} = 0.76 \times 10^{-2}$ and a percentage deviation of 22.6%. Values of k for Al_2O_3 obtained from other sources[5] are

k = 1.363 x 10^{-2} at 1291°K and k = 1.33 x 10^{-2} at 1400°K and for graphite at 1189°K, k = 0.1020. The deviations of the average experimental values of k for Al_2O_3 from the values obtained from the literature[5], referred to an average, are 2.8% and 16.1%. For graphite the corresponding deviation is 14.5%

D. SUMMARY

Values of c$_p$ for α measured at the smallest values of τ are shown in Tables VIII and IX. Density was calculated from a measure of mass and sample dimensions. Emissivity was taken from Figures 24 25 and 26 Values obtained from other sources[5] are listed as "Other Values".

Measurements were taken in a range of βl where the sine wave phase shift was decreased by a factor of 24% to 40% over that predicted from ϕ = βl. The difference in power radiated in this range (βl<1 rad), ΔPr, was in error by as much as 7.5% by the neglect of 2nd order and higher terms. Because the order of magnitude of h was 10^{-3} cal/cm^2 sec °K, this error produced no significant error in ϕ.

TABLE VIII

Thermophysical Properties of P.C. Al_2O_3
$\rho = 4\,gm/cm^3$ $K = 0.147$

$\overline{Ta}_s$	$\overline{k}(cal\ sec^{-1}\,cm^{-1}\,{}^{o}K^{-1})$	$\alpha(cm^2\,sec^{-1})$	ϵ	$C_p(cal\ gm^{-1}\,{}^{o}K^{-1})$
1290	0.0141	0.0067	0.684	0.52
1400	0.01675	0.0096	0.83	0.43
Other Values[5]				
1290	0.0136	0.0117		0.31
1400	0.0133	0.0104		0.32

TABLE IX

Thermophysical Properties of Graphite,
$\rho = 1.51\,gm/cm^3$ $K = 0.147$

$\overline{Ta}_s$	$\overline{k}(cal\ sec^{-1}\,cm^{-1}\,{}^{o}K^{-1})$	$\alpha(cm^2\,sec^{-1})$	ϵ	$C_p(cal\ gm^{-1}\,{}^{o}K^{-1})$
1189	0.0829	0.0854	.93	0.64
Other Values[5]				
1189	0.102	0.147		0.43

For values of $\beta1 = 1.6$ rad, and $k = 0$, the tan ϕ deviates by 8% from

tan $\beta1$ and ϕ converges rapidly to $\beta1$ as $\beta1$ increases. By the use of more

sensitive radiometers and by presenting the radiometer outputs together

on an oscilloscope, more accurate determinations of ϕ can be made.

Determination of these values from photographs and tapes was difficult.

V. DISCUSSION AND CONCLUSIONS

There are several limitations in the electron bombardment technique but these are outweighed by the numerous advantages. The major advantage is that all of the thermophysical properties of a particular material can be measured over a wide temperature interval (up to the melting point). An independent determination of the emissivity was made in the experiment just described. The accuracy of such a measurement is determined primarily by the accuracy with which temperature can be measured. The principal shortcomings of the system will be discussed first.

The principal disadvantage lies in the fact that the sample material must not decompose in a vacuum (i. e., must not have a high vapor pressure) and must not have an excessive electrical resistance. The latter condition can be overcome by coating the surface of the sample specimen, but this introduces a change in surface emissivity. The low vapor pressure requirement is met by most high-temperature materials so that a very large class of materials lend themselves to this technique. This vapor pressure limitation is also inherent in other techniques used to measure thermophysical constants.

A sine wave is just one of many boundary conditions that can be employed in the electron bombardment technique. For example, saw-tooth functions, parabolic functions, etc., could be used. Since electronics is a very highly advanced form of technology, these power

inputs, as well as the parameter measurements, can be made more reproducible than by other techniques.

As a result of the above discussion, it must be concluded that this technique becomes very practical at high temperatures (where $T \gg \theta$) and for $\beta l > 1.6$ rad. The accuracy with which the values could be repeated was good. Consequently, the results of the experiment indicate that, with better instrumentation, more accurate results can be attained with this technique.

It is concluded that the most important advantages of the electron bombardment technique lie in the fact that any desired rate of heat energy input to the sample can be attained and that there is no theoretical limitation on the temperature. This energy deposition rate can take any desired functional form and can be applied to a wide variety of shapes, such as spheres, cylinders, disks, etc. Consequently, the technique represents a versatile method for measuring the thermophysical properties of materials.

VI RECOMMENDATIONS

The desired characteristics are as follows:

A.   The apparatus should be capable of delivering sufficient power to heat any required sample size of any material to its melting points.

B.   Provisions should be made for varying the power according to any desired functional form.

C.   Provisions should be made either for determining the temperature of the sample or for determining its emissivity by an independent means.

D.   A vacuum system having sufficient capacity to lower the pressure rapidly within the chamber should be provided in order to eliminate the delays caused by outgassing of the sample while it is being heated.

E.   A method for focusing and bending the electron beam is needed so that the reflection of light from the filament is eliminated.

F.   Provision for mounting the radiation sensors internally to eliminate transmission problems through the viewing ports is required.

A.   POWER REQUIREMENTS

The use of a variety of samples requires that the power input must be capable of supplying sufficient heat in the most extreme case

which is anticipated. If an upper limit on the temperature is 4000°K, since the upper limit on the emissivity is unity, the upper limit on the power radiated per unit area is 1450 watts/cm^2. A reasonable sample shape could be a cylinder having the two faces to side area ratio, (1/r) equal to or less than 0.1, where 1 is the length and r is the radius of the cylinder. Since relatively high thermal conductivities may be encountered in samples of interest, a value of 1 $\cong$ 0.3cm would probably be required to give sufficiently large phase shifts for accurate determinations of α. Thus, the total sample plus whatever guard ring type of device that might be used around the sample may be required to be as large as 60 cm^2. This coupled with the 1450 watts/cm^2 upper limit on the radiation gives a power requirement of about 90 kw. In order to assure that the resulting apparatus will be capable of handling any known high temperature material, it is recommended that the power supply be capable of delivering 100 kw of power.

B. BEAM CONTROL

Precise control of the power input must be instituted if accurate forms of heat waves are to be generated at the sample surface. Since it may be desirable to vary the rate of heat energy input with respect to time over a wide range of functional forms, it is recommended that the beam power be controlled by use of a function generator. That is, the radiometer output while viewing the sample should be compared with the function generator signal and the difference amplified and used

to control the power input to the sample. In this way the heated sample face can be made to follow any desired functional form with respect to time (within the theoretical limitations discussed above).

C. TEMPERATURE OR EMISSIVITY DETERMINATION

The emissivity of a material can be related to the other thermophysical properties only through radiometer measuring techniques as discussed above. That is, the emissivity is not related to α, ρc_p, or k by any known physical laws even though they may be physically related. The parameters α, ρc_p, and k are relatable to the internal temperature behavior of a material through known physical laws. Thus they can be related to the emissivity only through a comparison of the apparent (radiation) and actual temperatures of the surface of a material. This can be done in two ways: by measuring the emissivity independently, which relates the apparent temperature of the sample to its actual temperature, or by measuring the apparent temperature of the sample and its actual temperature simultaneously while the other parameters are being measured.

The second method for determining the temperature of the sample can be accomplished by drilling a small hole in it in a direction perpendicular to the cylindrical axis midway between the two faces. Observation of this hole by means of a radiometer gives the actual temperature of the mid-point of the sample. Then from the steady state conditions the output of the two radiometers viewing the faces of the sample

can be converted to actual temperatures by reading of the mid-point temperature as follows. Let the actual temperature of the mid-point, as observed on the radiometer viewing the hole at the mid-point, be T_{as}. Then $(\frac{1}{2}) \varepsilon^{-\frac{1}{4}}(T_{Bf} + T_{Bb}) = T_{as}$ under equilibrium conditions. Thus, $\varepsilon = [(T_{Bf} + T_{Bb})/2T_{as}]^4$ is given directly by the three radiometer readings.

Although either one of these methods will give the correct results, they both have advantages and disadvantages. The first method discussed has the advantage that it gives the emissivity directly in terms of the definition of emissivity, but has the disadvantage that a separate measurement is required. The second method has the advantage that only one single experiment is required to obtain all four of the thermo-physical parameters; it has the disadvantage that three temperature measurement errors are involved in ε, whereas only two temperature errors are involved in ε when the former method is employed. It is recommended that either of these methods, or both, be employed to determine the very high (greater that 2300°K) temperature emissivities. For low temperatures (up to 2300°K) it is recommended that the temperature on the faces of the sample be measured directly by the use of thermocouples for determining the emissivity.

D. VACUUM SYSTEM

One of the time consuming aspects of performing the measurements involves waiting for the vacuum system to overcome the

outgassing of the sample during heating. Consequently, it is recommended that the conventional vacuum system be supplemented by an ion pump.

E. FOCUSING OF ELECTRON BEAM

One of the problems encountered in making the measurements resulted from the filament light being reflected from the sample and the walls of the vacuum chamber into the sensing devices. This will not generally be a problem at very high temperatures, but at low temperatures where the sample emission is relatively weak it will be quite troublesome. This difficulty can be overcome by placing the filaments in such a position that they are not in the view of the sample. Consequently, it is recommended that the electron beam be magnetically focused through a 90 degree turn before it is allowed to strike the sample.

If the above recommendations are carried out the resulting apparatus will be capable of measuring the thermophysical parameters of all nonvolatile materials at high temperatures. It will also be capable of measuring these parameters for poor thermal conductors at low temperatures in accordance with the limits established by the instrumentation.

BIBLIOGRAPHY

1. Jakob, M., Heat Transfer, John Wiley & Son, 1958.

2. Menzel, D. H. (Edited by), Fundamental Formulas of Physics, pp. 261-262, Prentice-Hall, Inc., New York, 1955.

3. The International Dictionary of Physics and Electronics, VanNostrand Co., Inc., New York, 1956.

4. Ibid.

5. Rasor, N. S., and J. D. McClelland, "Thermal Properties of Materials", Atomics International, March 1957, pp. 31-32. (Values of k and c_p for graphite) WADC TR 56-400 Pt. I.

   Fieldhouse, I. B., J. C. Hedge and J. I. Lang, Measurement of Thermal Properties, Armour Research Foundation, November 1958, pp. 18 and 41. (Values of k and c_p for Al_2O_3) WADC TR 58-274.